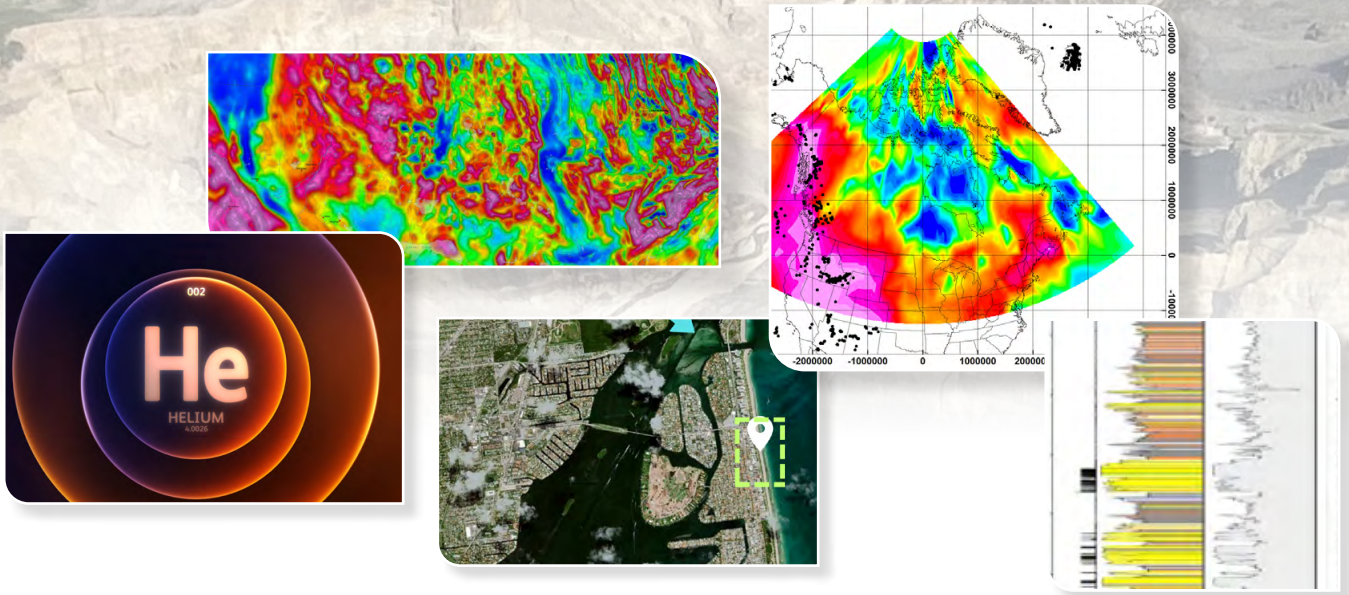# Reservoir

CEGA

cspg.org

THE 31ST ANNUAL

MIXED GOLF TOURNAMENT

Back after a 3 year absence, join us at the Lynx Ridge Golf Course for a four-golfer, best ball tournament!

Registration includes a round of golf, lunch, dinner and prizes!

AUGUST 23, 2023 | 1 PM
LYNX RIDGE GOLF COURSE

In This Issue

CONFERENCES

EVENTS

ALLUVIAL FAN, NORTHWEST TERRITORIES

This unnamed stream has created a 3.5 km-wide fan as it exits its confining canyon in the Mackenzie Mountains, carving into Paleozoic carbonates, and debouches northeastward through the mountain front. The stream joins other mountain-front drainages in the upper left and they ultimately flow into the Carcajou River to the northeast. The abrupt transition occurs approx. 60 km WSW of Norman Wells. The primary river channel within the fan has shifted laterally throughout time and is currently at the southern edge of this wedge of sediments. Scalloped erosional scarps characterize the margins of the upstream gorge.

Photo by: Wayne Laturnas

FROM THE EDITOR

SARAH SCHULTZ, TECHNICAL EDITOR FOR THE RESERVOIR

WELCOME
TO THE JULY/AUGUST ISSUE OF THE CEGA RESERVOIR!

In this issue we have the continuation of some of our regular articles:

- E.R. Crain's part 7 of the Petrophysics in the Green Economy series
- From the Desk of the AER: Strengthening the Alberta Advantage – Magnetic and Gravity Surveys
- Geology in Motion: Tom Brady and the Value of a Sand Grain

We present the following technical articles:

- J. Sellars et al: Mapping the 450°C Isotherm: Exploring the Potential of Deep, Super Hot Geothermal in Canada
- A. Tatomirovic: Canstrat Data and the Seamless Unison of Machine Learning

Congratulations to the presentation winners for the 2023 CEGA Core Conference:

- Pemberton Award (Best Overall Presentation): Joel Collins and Pak Wong
- Baillie Award (Best Student Presentation): Drew Brown

Please refer to the CEGA website for up-to-date information on upcoming division talks, conferences, and technical webinars.

Early Bird Registration for the 2023 Gussow Conference in Banff is now open! We hope to see many of you there taking in the technical presentations and networking events.

We look forward to continuing to receive your manuscripts for our remaining 2023 Reservoir Editions!

Sarah Schultz

BOARD OF DIRECTORS 2023

PRESIDENT
Simon Haynes
Haynes Geological Consulting
simon.haynes@cspg.org
LinkedIn

PAST PRESIDENT
Kelty Latos
ConocoPhillips Canada Ltd.
pastpresident@cspg.org
LinkedIn

PRESIDENT ELECT
Andrew Vogan
ConocoPhillips Canada Ltd.
presidentelect@cspg.org
LinkedIn

FINANCE DIRECTOR
Kathy Diaz
Krux Analytics Inc.
directorfinance@cspg.org
Linkedin

FINANCE DIRECTOR ELECT
Scott Norlin
Wood Mackenzie
directorfinanceelect@cspg.org
LinkedIn

DIRECTOR
Nicholas Ayre
Strathcona Resources Ltd.
conferences@cspg.org
LinkedIn

DIRECTOR
Mark Caplan
Imperial Oil
technicaldivisions@cspg.org
Linkedin

DIRECTOR
Ross Kukulski
Chevron Canada
publications@cspg.org
LinkedIn

DIRECTOR
Marcelina Labaj
Central European Petroleum Ltd.
fieldtrips@cspg.org
Linkedin

DIRECTOR
Shelley Leggitt
Kiwetinohk Energy Corp.
education@cspg.org
LinkedIn

DIRECTOR
Michelle Thoms
Freehold Royalties Ltd.
outreach@cspg.org
Linkedin

DIRECTOR
Valentina Vallega
Schlumberger
membershipdirector@cspg.org
Linkedin

CEGA

CEGA OFFICE
#150, 540 - 5th Ave SW
Calgary, Alberta, Canada T2P 0M2
Tel: 403-264-5610 | www.cspg.org

OFFICE CONTACTS

MEMBERSHIP INQUIRIES
Tel: 403-264-5610
Email: membership@cspg.org

ADVERTISING INQUIRIES
Britney Tang
Tel: 403-513-1230
Email: britney.tang@cspg.org

CONFERENCE INQUIRIES
Shaelyn Brown
Tel: 403-513-1238
Email: shaelyn.brown@cspg.org

MANAGING DIRECTOR
Emma MacPherson
Tel: 403-513-1235
Email: emma.macpherson@cspg.org

He

PART 7

HELIUM:
OLD WELLS ARE NEW AGAIN

E.R. CRAIN, P.ENG.

INTRODUCTION

The inert, or noble, gases comprise helium, neon, argon, krypton, xenon, and radon, of which helium is probably the most important. These gases are formed during the natural radioactive decay of elements such as uranium and thorium within the interior of the Earth and migrate upward to become trapped in porous rocks in sedimentary basins, usually in association with nitrogen and carbon dioxide. The helium content of these rocks seldom exceeds 7% by volume, but as little as 1% or even less can be economic.

Petrophysics plays an important role in defining porosity and gas saturation, but the porosity estimate is tricky because the gas correction implicit in the usual log analysis models fails to account for the lack of hydrogen in the gas. Solutions are provided, including examples.

Helium is a valuable inert gas used in commercial, military, and medical applications. It doesn't burn or combine chemically with other elements. It has unusual cryogenic properties and is used in welding to cool material adjacent to the weld and to cool the magnets in MRI machines, as well as the magnets at CERN that helped discover the Higgs boson. It also fills kids' balloons, weather balloons, dirigibles, makes your voice go squeaky when you breathe it, and helps spaceships get off the ground.

Helium and other inert gases are often found in conjunction with carbon dioxide and nitrogen and in wells that were originally drilled for oil or natural gas as early as 1903 (in Kansas). This discovery led to the development, by the US government, of a large helium resource stretching from Kansas through Oklahoma into the panhandle of Texas. Pipelines, separation facilities, and a large strategic reserve storage facility were built during the 1950s and 1960s. Some processing was privatized in the 1960s and private development was permitted from the 1990s. Canada and Poland produced small quantities in the 1960s and 1970s.

Today, the USA produces about 55% of global supply, Algeria and Qatar about 40%, with the remaining balance from a half dozen other countries. The price is a little volatile, averaging around US\$ 100 per thousand cubic feet (mcf), compared to natural gas at approximately US\$ 4.00. Gas analysis reports from helium bearing wells show high concentrations of CO_2 or N_2 with traces to several percent helium. Some have hydrocarbon gases (methane, ethane, propane) in quantities too small to allow the gas mixture to burn. A typical analysis might show 5% He and 95% N_2, or 5% He with 95% CO_2, or 5% He, 35% methane, with 60% N_2. Wells with less than
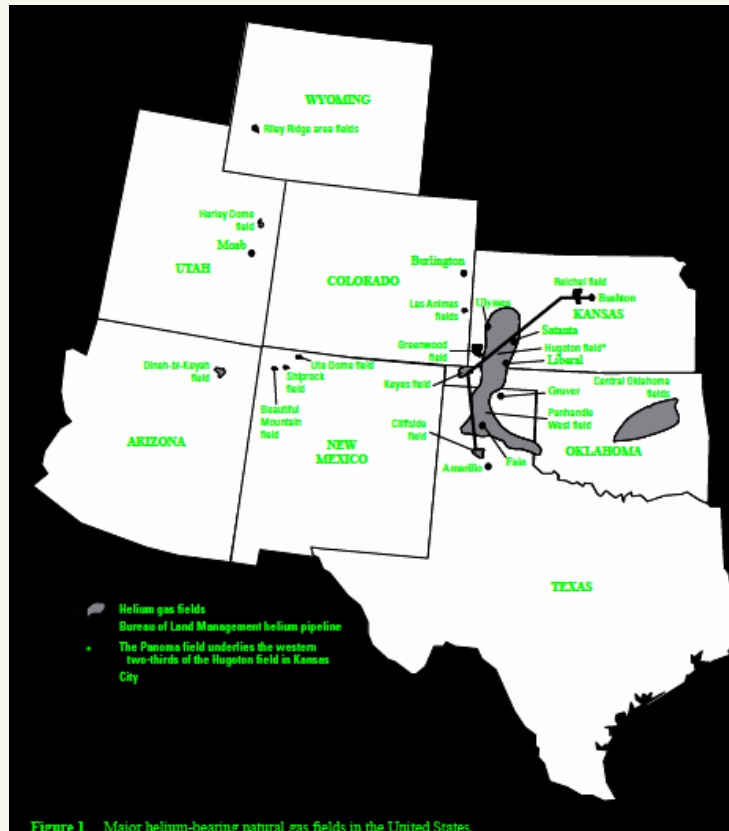
0.5% He are probably uneconomic; an average producing well in the USA has about 4% He. The method used to separate helium from a gas mixture is fractional distillation to create crude helium, followed by low temperature liquefaction to produce Grade-A 99.995% pure helium.

The major source of helium is radioactive decay of uranium and thorium in basement rocks or shales below potential reservoirs. Many helium producing fields are associated with volcanic intrusions or deep-seated basement shears. Some helium may also come from the primordial lithosphere through faults; this is the lighter isotope of helium. Few isotope ratios have ever been performed so the source is not precisely known in many cases. To trap helium in a reservoir you need the same geological setting as for natural gas: source rock, migration path, porous reservoir rock, structural or stratigraphic trap, and a seal at the top of the trap.

The migration path is usually through faults or fractures but could be via direct contact of a reservoir with a source rock. Reservoirs are usually sedimentary strata, but some igneous rocks may be porous and permeable enough to hold helium.

Traps are often structural, such as drape over domes or anticlines. Stratigraphic traps are harder to seal. The seal is more critical than for conventional oil or gas. The helium molecule is about half the size of a methane molecule so it can penetrate through smaller pores and fractures than methane. This makes the helium difficult to contain in samples and the seal on any trap must be lower permeability than a similar trap for oil or natural gas. The best seals are salt, salt plugged porosity, lava flows, or very fine claystone (shale).

Production rates vary with reservoir quality, thickness, and pressure. Many were overpressured and blew out in the early days of helium exploration. CAUTION: If you find production rates or production rate graphs, be sure to distinguish between total flow rate of all gases versus helium flow rates -- it isn't always clear.

If you are concerned about the environment, the inert gases, other than helium, are vented to the atmosphere, including CO_2 and any hydrocarbons in the mixture. A few wells are actually completed to capture CO_2 or N_2 for commercial purposes, but most are not.

Figure 1. Major helium-bearing natural gas fields in the United States.

LOG ANALYSIS IN HELIUM WELLS

Petrophysical analysis of inert gas reservoirs involves the same steps as any other gas well: shale volume, effective porosity, lithology, water saturation, permeability, and gas-in-place. There are a number of pitfalls in analyzing the well logs in helium bearing zones in addition to the usual problems of rough hole condition, highly variable mineralogy, salt plugged porosity, and varying water resistivity that can occur in any well. Here are the critical things that need to be considered:

1. Old wells have minimal log suites (Electrical survey [ES], possibly a microlog [MLC]). Wells drilled after 1960 may have a single transmitter sonic log; wells drilled after 1965 may have a density log, and if the Gods are willing, a gamma ray and neutron log (GRN), probably through casing. Each of these logs requires special handling, covered elsewhere in this Handbook, BUT ALSO subject to all the concerns listed below.

2. All porosity models must be corrected for shale volume. The gamma ray may permit this, but it should be calibrated to XRD clay volume on at least a few samples.

3. Inert gases have no hydrogen, so in theory the neutron log reads zero porosity. In air-drilled holes, there is no mud-filtrate invasion, so the neutron log reads near zero. On liquid-filled holes, the neutron log varies somewhat with the actual water saturation in the invaded zone and depth of investigation of the log. Clay volume, and whether or not the gas column contains hydrocarbon gas in addition to the inert gases, will increase neutron porosity. In some wells, invasion is deep enough for the neutron log to read a reasonable porosity value. In other wells, the neutron log reads zero or even slightly negative apparent porosity.

4. Sonic and density logs when transformed to porosity will read too high due to the gas effect, unless invasion is very deep and residual gas in the invaded zone is negligible (unlikely). Standard gas correction models will be needed,

FIGURE 2: Distribution of all known helium tests in the lower Paleozoic: Deadwood, Winnipeg, Red River and Stony Mountain formations. Image from "Helium in Southwestern Saskatchewan", Melinda Yurkowski, Saskatchewan Geological Survey, Open File Report 2016-1

calibrated to core porosity. Variations in matrix rock properties will need to be controlled by sample and core description.
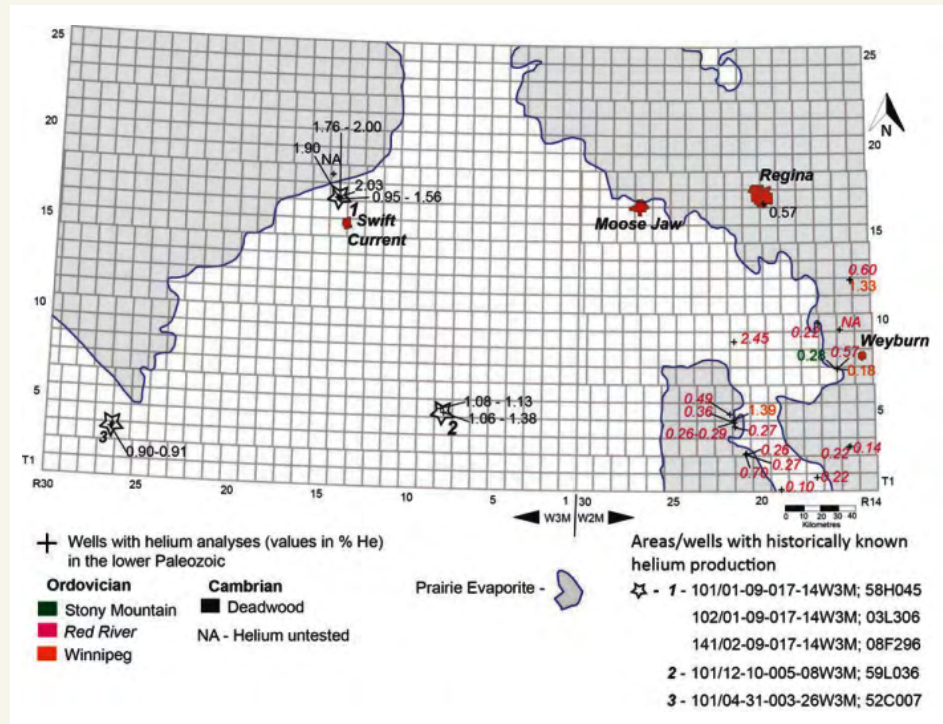
5. With the neutron log reading too low compared to a hydrocarbon gas (possibly near zero), the standard gas-corrected density-neutron complex-lithology model for porosity may not work well, giving a porosity that is too low. Some limited experience in Saskatchewan suggests that invasion may be sufficient to minimize this problem, but there was no core data available to prove this. In other project areas, the neutron reads zero and cannot be used as a porosity indicator.

6. NMR porosity is unaffected by clay, mineralogy, or gas effects, so it will give a reliable porosity in an inert gas reservoir, provided the borehole is not too rough and there is some drilling fluid invasion. Some core analysis control is comforting but less essential than for sonic and density porosity.

7. The only lithology model that works properly in a gas reservoir is the PE two-mineral model. The PE curve was not common until the 1990s and may be missing in many wells drilled after that date, so there may be no direct method to calculate mineralogy. Sample and core descriptions are a necessity to assist in understanding the mineralogy and the higher quality reservoir facies.

8. After a porosity algorithm has been calibrated to core, the deep resistivity can be used to calculate water saturation, provided the correct Rw regime can be identified. This allows the calculation of total gas in place. Multiply gas in place by helium fraction to obtain helium in place.

9. If salt plugging is present, it might be identified by a very high resistivity and very low neutron and/or NMR porosity. The efficacy will depend on whether the drilling fluid has dissolved the salt in the zone investigated by the neutron log. Sonic and density porosity may be lower than non-plugged intervals due to the different log response of salt and gas. Results may still be ambiguous. When identified, salt plugged zones are flagged and the porosity is set to zero.

10. Once porosity and saturation are calculated, and salt plugged intervals are flagged, permeability can be calculated from the usual Wyllie, Timur, or Lucia methods. An estimate of total gas deliverability at initial unstimulated conditions is possible based on the sum of permeability thickness values. There is a large possible error in this result as natural fracture permeability is not included.

11. Helium concentration CANNOT be calculated directly from any well log result.

12. Inert gas wells are among the most difficult to quantify using well log data. Core analysis data and sample descriptions, with a little help from XRD mineralogy data, can make the results a little more conclusive. Commercial software will most likely fail to give an accurate estimate of porosity unless you add some user-defined equations to account for the peculiar gas effect caused by inert gases.

LOGGING PROGRAM FOR INERT GAS WELLS

While we are stuck with the log suite in existing wells, we can run an appropriate program today that will give optimum results. The recommended suite is:

1. Array induction or array laterolog with SP and gamma ray (in air-drilled holes, laterolog cannot be run).
2. Density neutron with PE and spectral gamma ray.
3. Nuclear magnetic resonance log with gamma ray.
4. Array sonic log for correlation with older wells and to assist seismic interpretation.
5. Resistivity image log to assist in facies description, and trap and seal definition.

Items 3 and 5 are needed only from TD to 100 meters above the zone of interest.

Gas log, conventional or drilled sidewall cores, closely spaced sample description, and XRD mineralogy and bulk clay are strongly recommended.

LOG ANALYSIS EXAMPLES IN HELIUM WELLS

1. ANCIENT LOG EXAMPLES WITHOUT QUANTITATIVE PETROPHYSICAL ANALYSIS (See Figure 3)

These two examples are from "Oil and Gas; and Helium Production Potential of Oil and Gas Assets in Navajo County, Arizona" by Olufela Olukoga, prepared for Blackstone Exploration Company Inc.

2. MODERN PETROPHYSICAL ANALYSIS EXAMPLES

These examples are from wells that have tested or produced inert gas with helium in economic quantities. The analyses were performed for North American Helium Ltd. and are reproduced here with their permission.

EXAMPLE 1: Air-drilled Inert Gas Well (See Figure 4)

EXAMPLE 2: Liquid-filled Borehole (See Figure 5)
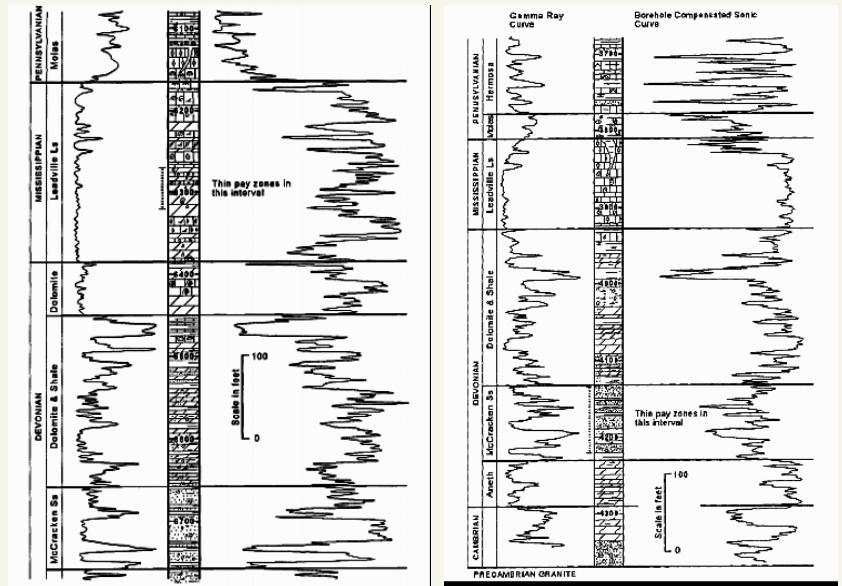
FIGURE 3: Left: Ancient gamma ray neutron log in helium bearing reservoir in the Tohache Wash Field. Gas in the Mississippian was 6.03% helium. Cumulative production was 385 Bcf total gas. Neutron deflections to the right are low porosity OR inert gas. Right: Borehole compensated sonic log in Kerr-McGee #2 Navajo-C well showing the stratigraphic position of the helium-bearing reservoir in the Dineh-bi-Keyah Field. Gas in the Devonian ranges from 3.11% to 6.23% helium and averages 4.83% helium; the zone produced 1.4 Bcf total. High sonic travel time is high porosity or shale.
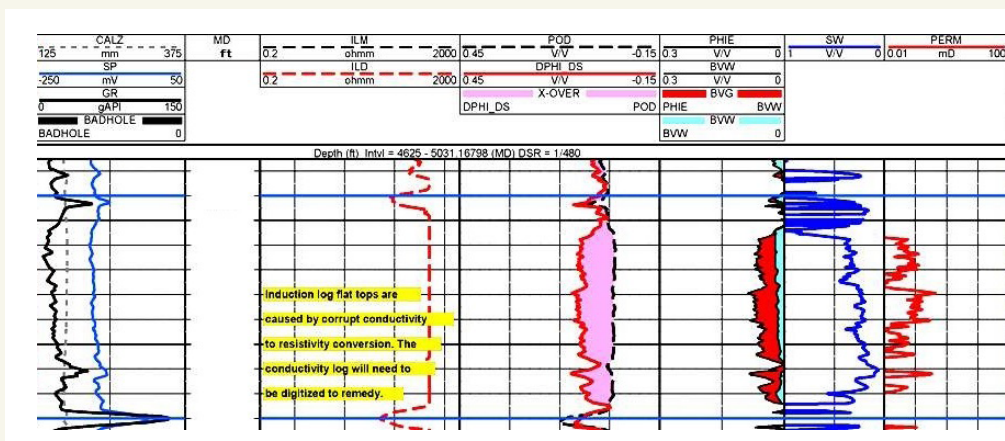
FIGURE 4: From left to right the tracks contain gamma ray, deep resistivity, density, neutron (with gas crossover shaded pink), effective porosity (with inert gas volume shaded red), water saturation, and permeability curves because inert gas has no hydrogen content and there is no invasion from a liquid borehole fluid. SP, shallow resistivity, and sonic are missing because they cannot be recorded in an air-drilled hole.
(Image courtesy NA Helium).

FIGURE 5: From left to right the tracks contain gamma ray, deep and shallow resistivity, density, neutron (with gas crossover shaded pink), calculated effective porosity (with inert gas volume shaded red), water saturation, permeability, and lithology curves. Neutron log responds to invasion water but may read a bit low due to residual inert gas in the invaded zone. *(Image courtesy NA Helium)*.

ACKNOWLEDGEMENT

REFERENCES

1 Inert Gas Technical Data Various Wikipedia pages, 2022.

From the Desk of the AER

Dinu I. Pană – Alberta Geological Survey, Calgary
Henry Lyatsky – Consultant, Calgary
Rastislav Elgr – Alberta Geological Survey, Edmonton

STRENGTHENING THE ALBERTA ADVANTAGE

Over 70% of the province is covered by new public-domain, high-quality airborne magnetic and gravity surveys

Rationale

Public-domain regional maps and other geoscience data are a typical starting point for mineral and hydrocarbon exploration. Magnetic and gravity data can be used jointly with other geophysical data and geologic field mapping and drilling to identify rock types as well as potential faults and fractures in the subsurface.

Generation and public dissemination of geoscience data and map products in advanced nations had historically been the mandate of provincial and national geological-survey agencies. As part of the Alberta Minerals Strategy, between 2021 and 2023 the Alberta Energy Regulator (AER) and the Alberta Geological Survey (AGS) carried out the largest high-quality regional airborne magnetic and gravity survey in modern Canadian history, and one of the largest worldwide.

Previous regional public-domain geophysical data

To the discouragement of exploration investors, much of the old public-domain magnetic and gravity coverage in Alberta is archaic, sparse, or entirely non-existent. For example, much of the publicly available old magnetic data in northern Alberta were flown as far back as the 1950s, with extremely sparse line spacing and long before the introduction of modern recording and positioning capabilities. Still, these old data sometimes provide useful calibration for interpreting the new data (Sprenke et al., 1986). The old gravity data were recorded on land, with stations in northern Alberta sometimes many tens of kilometres (km) apart.

The maps were produced by digitizing old contour maps donated by petroleum companies or recorded by government agencies and interpolated onto a 2-km grid. Unfortunately, a large area in north-central Alberta had never been covered by public-domain aeromagnetic surveys at all.

New data acquisition – survey design

The recent survey coordinated by the AGS involved four specialist companies that employed multiple fixed-wing aircraft equipped with state-of-the-art instrumentation. This regional survey encompassed multiple areas with very different magnetic grains, and the flight-line orientation was set to run across the dominant magnetic grain in each anomaly domain. This new Alberta survey acquired geophysical data for nearly 800,000 line kilometres (lkm; 732,422 lkm newly flown and 66,539 lkm purchased) of magnetics and ~134,000 lkm of gravity. Excluded were areas near the Rocky Mountains and Foothills where the low-level flying conditions were deemed unsafe, the restricted airspace over the Cold Lake airbase, and some urban areas with a lot of magnetic infrastructure. Gravity was flown concurrently with magnetic data, using the same aircraft equipped with both types of recording instrument.
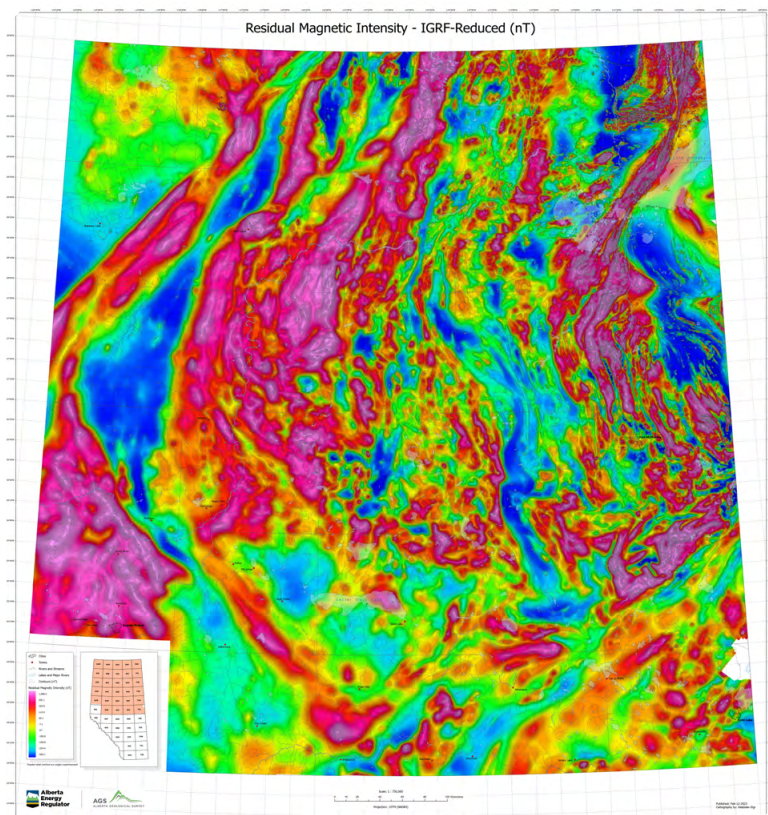
Residual Magnetic Intensity - IGRF-Reduced (nT)

The magnetic data, with a 200 m terrain clearance, flight lines spaced at 800 m and tie lines at 2,500 m, cover 31 NTS map sheets over the entire northern Alberta Plains between the latitudes of 54°N and 60°N (Figure 1), for a total of 573,682 lkm. The roughly N-S magnetic grain in the north-central Alberta Plains required E-W flight lines, whereas the NW and SE parts of the survey area were covered by NW-SE flight lines, orthogonal to the underlying Great Slave Lake and Snowbird tectonic zones and associated features. Many of the data-acquisition and -processing details are given by Lyatsky et al. (2022). Selected areas of inferred prime mineral potential, such as the NE-trending "kimberlite corridor" in north-central Alberta and the Hay River Fault zone in NW Alberta, were also given air gravity surveys.

The Canadian Shield in NE Alberta, where many anomaly sources lie at the surface, received high-resolution aeromagnetic coverage with a 400 m line spacing and a 2,500 m spacing for tie lines, with a 100 m terrain clearance, for a total of 52,205 lkm.

The southern Alberta Plains between the Montana border and 51°N (4 NTS sheets) were covered with magnetic data flown with an 800 m line spacing and tie lines at 2,500 m, with a 200 m terrain clearance, totaling 106,535 lkm. Here too, flight-line orientation was varied to run across the dominant magnetic anomaly grain: the northern block was flown N-S, orthogonal to the Vulcan structure, whereas the southern block was flown E-W, orthogonal to the dominant magnetic grain in the Medicine Hat basement.

The newly acquired data were decultured, leveled, gridded, and processed to generate a suite of derivative maps. Our data processing generally followed the practices used successfully in the oil and mining industries and by the AGS in the past to enhance subtle anomalies of potential exploration significance. Still, a good deal of experimentation was needed to generate the derivative maps with maximum interpretation value and to reduce noise.

Reduction of the magnetic data to the pole was avoided because it assumes that all the anomaly-causing rock magnetization is induced and the remanence is zero; on a regional scale, such an assumption is highly likely to be false, and rocks in the Canadian Shield in NE Alberta are indeed known to carry remanent magnetization (Sprenke et al., 1986). Besides, Alberta lies at a fairly high magnetic latitude, where changes to the data from pole reduction tend to rather small (Pilkington et al., 2000).

The AGS is using these high-quality new data to create maps, update the Alberta Interactive Mineral Map (AIMM) viewer, and interpret rock composition and possible shear zones and fractures in the subsurface. The grids are provided to the public in both Geosoft and ASCII formats, so they can easily be imported into a variety of mapping packages. If the users wish to process these data beyond the derivative products and map displays we provide, they are able to do so with the supplied grids.

Significance of magnetic and gravity anomalies

Magnetic anomalies delineated in our regional survey are sourced overwhelmingly in the crystalline basement. Depth to basement in north-central Alberta increases greatly from NE to SW. Small intra-sedimentary and near-surface sources of magnetic anomalies occur sporadically in the Alberta Basin, related to local occurrences of igneous rocks such as some kimberlite pipes in north-central Alberta and the Eocene dikes and volcanics in southern Alberta, and intraformational primary or secondary mineralization. The usual assumption that the Alberta Basin is essentially magnetically transparent holds in most areas.

Near-surface magnetic noise was caused by fluvial erosion, magnetic glacial erratics, and most of all, by man-made infrastructure. Some of the ongoing industrial activity even made the cultural noise time-variant. Manual and automatic deculturing, as well as anti-aliasing with

the Hanning convolution filter, helped to reduce this noise substantially. Drainage has an undesirable potential-field signature where rivers cut valleys into the glacial till, but the choice of a low Bouguer density (2.10 g/cc, to match that of the till) greatly reduced this type of noise in the gravity maps. Where the till composition happens to make it magnetic, drainage appears vividly in the derivative magnetic maps.

Magnetic anomalies typically indicate lateral variations in rock mineralization related to variations in protolith composition, metamorphic patterns, and structural deformation. Gravity anomalies arise due to lateral variations in the bulk density of rocks. Large and broad anomalies are typically related to metamorphic and igneous rocks' geologic grain and ductile deformation, whereas sharp but subtle discontinuities are sometimes associated with brittle faults (e.g., Schulte et al., 2019). High-quality aeromagnetic and gravity data can provide information relevant to:

- geologic mapping and structure delineation
- petroleum exploration
- mineral exploration
- critical-commodity exploration
- groundwater development and conservation
- earthquake-hazard assessments

Mineral and oil exploration across Alberta, including exploration for commodities that are newly critical to the economy and to national and Allied security, will benefit from having the province remapped with these new surveys. With better public-domain data, this remapping will make Alberta a more attractive destination for exploration investment.

Future anomaly analysis can also lead to better definition of anomaly domains in the western Canada crystalline basement. These anomaly domains can then help to refine our understanding of geologic and tectonic crustal domains on a regional scale.

References

Lyatsky, H., Pană, D., Moussaoui, K., Cortada, C. and Elmoussaoui, S., 2022. New regional aeromagnetic surveys in northern Alberta; Recorder (Canadian Society of Exploration Geophysicists), v. 47, no. 1.

Pilkington, M., Miles, W.F., Ross, G.M. and Roest, W.R., 2000. Potential-field signatures of buried Precambrian basement in the Western Canada Sedimentary Basin; Canadian Journal of Earth Sciences, v. 37, p. 1453-1471.

Schulte, B.W., Bridge, D. and Lyatsky, H., 2019. Methods of fault detection with geophysical data and surface geology; Recorder (Canadian Society of Exploration Geophysicists), v. 44, no. 5.

Sprenke, K.F., Wavra, C.S. and Godfrey, J.D., 1986. Geophysical Expression of the Canadian Shield in Northeastern Alberta; Alberta Geological Survey, Bulletin 52, 54 p.

THE 2023 GUSSOW CONFERENCE:

Geomechanics for Sustainable Energy Development

By Amy Fox, Gussow Planning Committee Chair

Another Gussow Conference will be held in beautiful Banff, Alberta this October 10-12, and the theme this year is geomechanics! The planning committee, consisting of myself, Chris Hawkes, Pat McLellan, Doug Schmitt and Baohong Yang, has put together a fantastic line-up of talks on a wide range of geomechanical topics from oil and gas, geothermal, carbon storage, and nuclear waste disposal. Speakers will be coming from companies, universities, geological surveys and research organizations in Canada, the U.S. and Europe. I encourage interested readers to take a peek the detailed technical program, which is already online (even though a few details are subject to change as the planning wraps up).

GUSSOW 2023
Geomechanics for Sustainable Energy Development
Banff, AB | October 10-12

Geomechanics has, of course, been an integral component of our energy system for a long time, but now its role in the energy transition is coming to the fore. Many of the same concerns apply, including the safe drilling of wells, caprock and wellbore integrity, induced seismicity and others. Geomechanics will be critical for the success of early projects that will pave the way for our energy future. As always, the 2023 Gussow Conference will be a uniquely focused, single-track event with abundant opportunities to learn from and interact with a community of individuals with shared interests and concerns. We're planning some exciting social events including an Icebreaker reception at the Cave and Basin National Historic Site and a lunchtime field trip. There are also opportunities for students to present posters and sponsors to interact directly with delegates. Be sure to register and book your room early to guarantee your spot. We hope to see you in Banff!

Sessions

SESSION 1: **In-Situ Stresses with Applications to Petroleum and the Energy Transition**

This session will highlight both long-established workflows and some of the great strides that have been made in recent decades in the methods used to measure stresses and interpret them at a variety of scales from the wellbore to the geological basin.

SESSION 2: **Geomechanical Characterization of Rock and Fracture Properties**

This session will discuss the characterization of intact rock and natural fractures using laboratory testing techniques and geophysical logging, highlighting new measurement tools and techniques as well as presenting comprehensive case studies.

SESSION 3: **Geomechanical Issues and Applications Associated with Injection and Storage**

This session will discuss some of the geomechanical issues/applications associated with injection and storage in geological formations, such as: stress or rock property changes, experimental analysis, modelling, and field studies.

SESSION 4: **Natural Geomechanical Subsurface Hazards and Risks: Characterization and Assessment**

This session will highlight case studies where some knowledge of geomechanical risk was present at the beginning of a project. The focus will be on how that risk was characterized and assessed, and how approaches to risk characterization and assessment, or the risk itself, may have changed over time.

SESSION 5: **Evolving Stress Conditions: Measuring and Monitoring**

This session will focus on tracking, directly or indirectly, natural and anthropogenic changes in stress fields, fault motions, and pore fluid saturation within the earth for optimizing efficiencies and guarding against induced hazards.

Mapping the 450°C isotherm: Exploring the potential of deep, superhot, geothermal in Canada

Josh Sellars – Seequent, Canada
Philip, J. Ball – CATF, USA
Kathleen Gould – Seequent, Canada
Juan Carlos Afonso – University of Twente, Netherlands

LithoRef18 computed depth to 450 degC
Black dots represent known volcanes
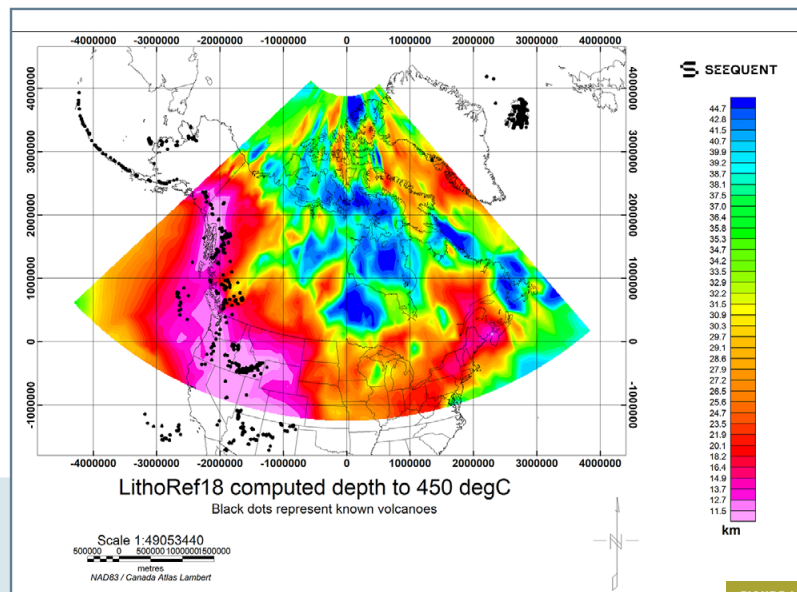
Scale 1:49053440

FIGURE 1

Theory

In the current global geo-political environment, many governments are looking towards alternative energy sources to assist with the phasing out of fossil fuels. As a result, geothermal energy has seen an intensification of interest because it provides cost-competitive, low-carbon, always available renewable energy, while requiring significantly less land than other energy sources. Increased exploration of geothermal resources is occurring in tandem with a boom in technological innovations, with an eye towards exploration of deeper and hotter geothermal resources.

To explore for supercritical geothermal resources, an improved understanding of subsurface temperatures and pressures is needed. Successful characterization of the depth to critical isotherms and potential resource density requires a better understanding of the thermal structure of the entire lithosphere, yet hard data to constrain these models remains sparse, leading to uncertainties in the global characterization of thermal anomalies.

Using global lithospheric models (LithoRef18, Afonso et al., 2019), we examine and compare the predicted surface heat flow models and the computed depths to critical isotherms. The results allow us to characterize the first-order nature of the thermal structure of the Earth's lithosphere and the geodynamic environment in which these thermal anomalies occur. In addition, we explore uncertainties in the depth and spatial location of the thermal anomalies between models and investigate the challenges of developing a thermal model that can be used for the delineation and estimation of next-generation, superhot rock geothermal opportunities.

Introduction

Prior to 1973 little was known about the geothermal potential of Canada (Jessop et al., 1991; Hickson et al. 2020). Fifty years later, our knowledge of the thermal structure of Canada has improved; however, only recently have we begun to construct geothermal power plants. At present, there are two power generation plants commissioned: in Saskatchewan, by Deep Earth Energy Production Corp, (Potkins, 2023) and in Alberta, by FutEra Power Corp. (Razor Energy, 2022). Several other projects are in the planning phase due to the increased awareness of the value of geothermal energy, particularly in Canada's decarbonization ambitions (Graham et al., 2022). Recent studies have provided information on the geothermal potential of Canada from depths of 50 m to 10 km (e.g., Grasby et al., 2009; Grasby et al., 2012), with Graham et al. (2022) arguing that 90% of the geothermal opportunity can be unlocked using engineered geothermal systems (EGS) technologies to reach deep geothermal resources at depths of greater than 5 km. Major barriers to delivering such projects include a better understanding of the geotherm coupled with complexities of drilling, completion and reservoir creation at the required depths. Continued innovation is rapidly breaking down many of the technical barriers, making geothermal available almost everywhere (e.g., Ball, 2021; Graham et al., 2022; CATF, 2022; Beard & Jones, 2023).
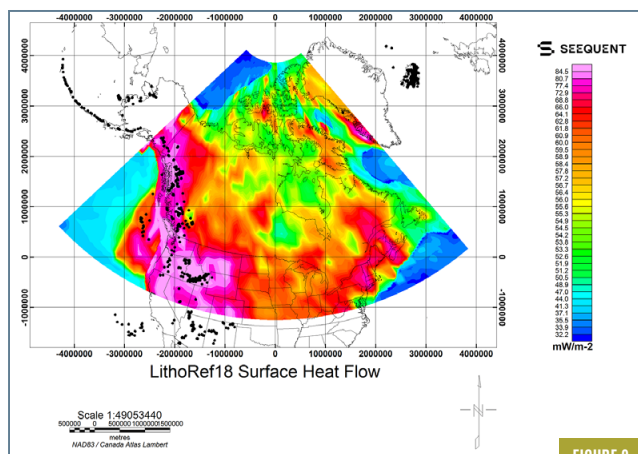
LithoRef18 Surface Heat Flow

Scale 1:49053440

NAD83 / Canada Atlas Lambert

FIGURE 2

Surface Heat Flow, Fuchs et al (2021)

Scale 1:49053440
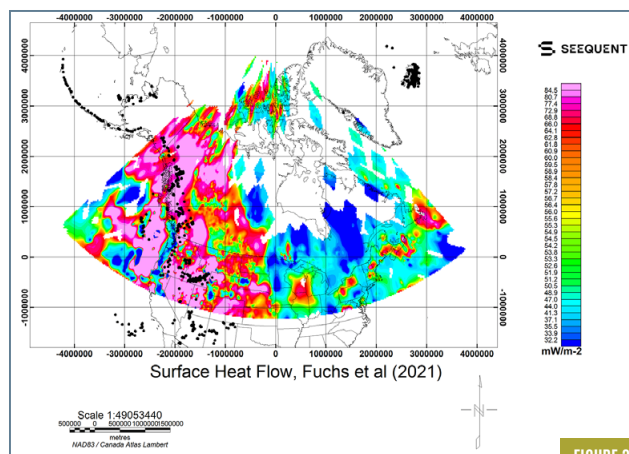
NAD83 / Canada Atlas Lambert

FIGURE 3

Several factors contribute to the source of the Earth's heat. A small component of the heat that we observe at the Earth's surface is derived from primordial heat, generated from the formation of the planet. The real engine, however, is the presence of naturally occurring, decaying radioactive isotopes like Potassium 40, Uranium 238, 235, and Thorium 232, which are contained within the Earth's crust and mantle. It is important to note that these elements are not uniformly distributed, which sets up a first-order heterogeneity of the Earth's mantle and crust. Furthermore, the heat generated does not stay in one place within the crust or mantle; it moves around, through processes such as conduction, advection, and convection. Hydrothermal systems are an important part of the heat transfer process from deep to shallow, forming convective cells within the shallow sections of the Earth's crust and sedimentary basins. Mantle convection and plate tectonics combine to largely dictate where we are likely to locate the heat deep in the Earth's crust. The concept of mantle convection allows for the large-scale convection of heat rising and sinking within the mantle. Convective and advective processes locally modify thermal conditions, particularly at new/forming plate boundaries or where mantle plumes or magmatic provinces form and modify the thermal conditions in the crust and lithosphere. Elsewhere, conduction forms the dominant way in which heat is transferred within the Earth's lithosphere and mantle.

Historically many of the world's early geothermal plants exploited hydrothermal dominated systems where hot water within the crust locally convects, bringing heat to shallow depths within the crust. To date, most of the early power plant developments tend to be located at divergent, convergent, or transcurrent plate margins, as indicated by the distribution of geothermal electricity generation plants (Uihlein, 2018). The hydrothermally derived geothermal power plants provide a skewed understanding of heat flow in the shallow crust, and they are geographically limited. With the concept of Engineered Geothermal Systems (EGS), it is possible to decouple the need for shallow hydrothermal systems and explore for hot rock, where thermal reservoirs can be exploited. Superhot rock forms the deepest, highest temperature geothermal resource opportunity, from a spectrum of opportunities at varying depth, and temperature, enabling the decarbonization of heating and cooling, electricity production and industrial processes. Clean water enters the supercritical phase at 22 MPa (220 Bar) and 374°C, and with increasing salinity the critical point also rises (CATF, 2022). Given the error in calculating deep geotherms and a limited understating of salinity of water in the crust, if present, we use a novel workflow to calculate the depth to 450°C from the LithoRef18 global lithospheric and mantle reference model to explore where superhot geothermal opportunities exist.

Focusing on Canada, using the resulting 450°C map, we aim to build an improved understanding of the depth to heat and explore building confidence on its spatial positioning. By improving our understanding of the distribution of deep thermal anomalies within the crust of Canada, we aim to move Canada one step closer to being able to successfully exploit and characterize its deep geothermal resources.

Method

The depth to the 450°C isotherm is calculated (Figure 1) using the 2°x2° global reference model LithoRef18 published by Afonso et al. in 2019. This global model was obtained through a formal joint inversion of 3-D gravity anomalies, geoid height, satellite-derived gravity gradients, and absolute elevation complemented with seismic, thermal, and petrological prior information. One of the forward problems solved during the inversion is the steady-state heat transfer in the lithosphere. In continental lithosphere, we solve the steady-state heat conduction equation with prescribed radiogenic heat productions and thermal conductivities dependent on the tectonic setting. In doing so, we subdivide the lithosphere into three layers: upper crust, lower crust, and lithospheric mantle where each layer has its own set of thermophysical parameters (see Afonso et al., 2019 for details). In oceanic domains, we compute the lithospheric thermal structure following the plate model of Grose & Afonso (2013) with crustal age from Müller et al. (2008). The onshore-offshore parameterization enables a seamless onshore-offshore product. The final thermal gradient in the continental crust is largely controlled by the lithospheric thickness and the internal heat generation in the crust.

Measured surface heat flow data was not used during the inversion. Predicted values of the long-wavelength surface heat flow by LithoRef18 (Figure 2) are, however, in close agreement with global observations in the Fuchs et al. (2021) Global Heat Flow Database (Figure 3), thus providing an independent validation of the model. For Canada, locally, the prediction of higher and lower surface heat flow is similar (Figures 2, 3, & 4). The fact that the long wavelength pattern of predicted and observed SHF match well indicates that the high-frequency anomalies in Figure 4 are likely of shallow origin.

Workflow

Using ESRI's ArcGIS and Seequent's Oasis Montaj software, we interrogated the calculated depths to deep thermal anomalies, derived from the LithoRef18 model (Afonso et al., 2018). We started this process by comparing the 450°C isotherm with temperature models from independent sources to understand if we can build confidence in the calculated depths returned from the LithoRef18 model. We also looked at the first order spatial relationships of the calculated depth to 450°C using the following workflow steps:

Comparison of depth to 450°C – using global Curie Depth Point (CDP) Models

Recently published global datasets are selected to be used to compare with the calculated results from the LithoRef18 model. In this study we access and compare the calculated depths from LithoRef18 to the following CDP models:

- Angulo and Vargas (2022), compute a global CDP model using the EMAG2v3 database. CDP modelling is completed using a centroid method (Angulo and Vargas 2022, see refs within),

- Li et al. (2017), compute a global CDP model using the EMAG2 database. CDP modelling is completed using magnetic anomaly inversion based on fractal magnetization.

- Gard and Jessop (2021), compute a global CDP model using the satellite lithospheric field model (LCS-1). CDP modelling is completed using an equivalent source magnetic dipole method.

This comparison, although instructive, needs to be taken with significant caution given the respective limitations and sensitivities of the different methods. In other words, it is valid to compare trends, but one needs to be cautious about the high-frequency discrepancies.

Spatial correlation of depth to 450°C with tectonic domain

We review the results of the LithoRef18 calculated depth to 450°C with geodynamic settings to observe a spatial pattern with tectonic domains from a model derived from Hasterok et al. (2022) We focus on the approximate tectonic age, plotting the basement rocks by their last orogenic event.

Spatial correlation of depth to 450°C with the location of conventional geothermal power plants and recent volcanics

We compare compilation of geothermal power plants from Uihlein et al. (2018) and known volcanoes from Ball et al. (2021) and Garrity and Soller (2021) to the results of the LithoRef model. We acknowledge that the spatial distribution of conventional geothermal power plants is biased towards hydrothermal and magmatic heat within the crust.

Observations

Comparison of depth to 450°C – using global Curie Depth Point (CDP) Models

When determining the predictive quality of our calculated depth to 450°C it is important to try to constrain the datasets against independent data. Due to the lack of wells that sample high temperature at depth that could be used for direct calibration, we are forced to compare our results to other independent models. To explore this idea, we set out to constrain our confidence in the calculated depth to the LithoRef 450°C isotherm. A test was conducted using temperature data derived from CDP models. Figure 5 reveals the calibration was not as straightforward as anticipated. We apply a simple colour scheme to show where LithoRef18 temperature results are shallower or deeper than CDP models (Figure 5). Blue areas show the calculated depth to 450°C is shallower than all CDP models, whereas the green, pink, and orange areas indicate that the LithoRef18 depth to 450°C is actually deeper than 1, 2, or 3 CDP models, respectively.

We took this analysis one step further to explore the average difference in depth (Figure 6a). Given the theoretical CDP is reporting a temperature of roughly 580°C, which is only 130°C hotter, the depth difference ought not to be too large. Even if a low geothermal gradient is assumed (e.g., 26°C/km) the bulk of the results should be within this error (e.g., +/-5 km). Figure 6a shows this is not the case. We can see the mean average difference can be quite large; in fact, it is larger than anticipated. Pinks indicate the LithoRef18 depth to 450°C
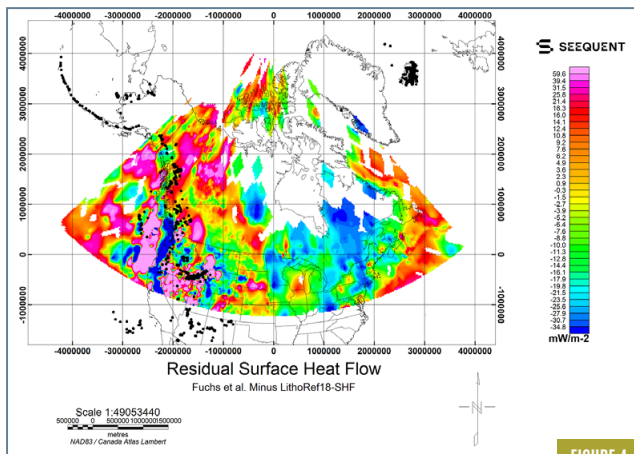

Residual Surface Heat Flow
Fuchs et al. Minus LithoRef18-SHF

Scale 1:49053440

metres
NAD83 / Canada Atlas Lambert

FIGURE 4

LithoRef18 depth to 450degC
Where shallower or deeper than Curie Depth Data

Scale 1:49053440

metres
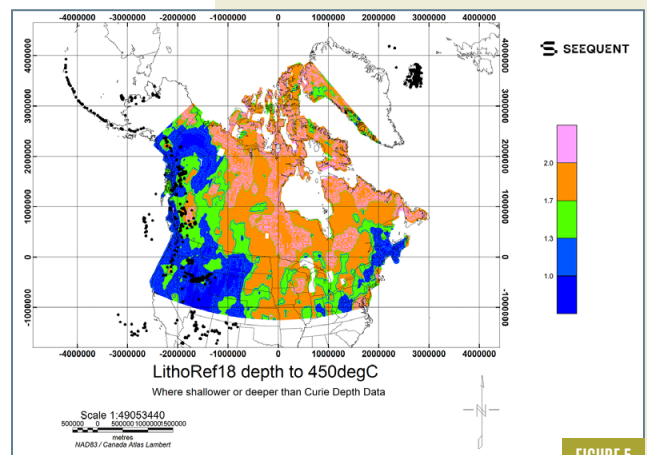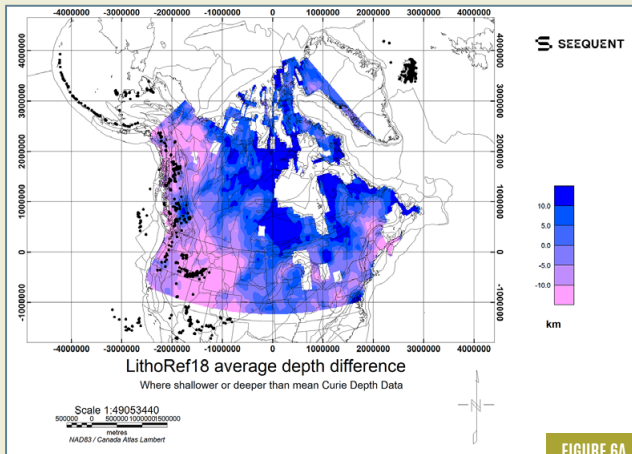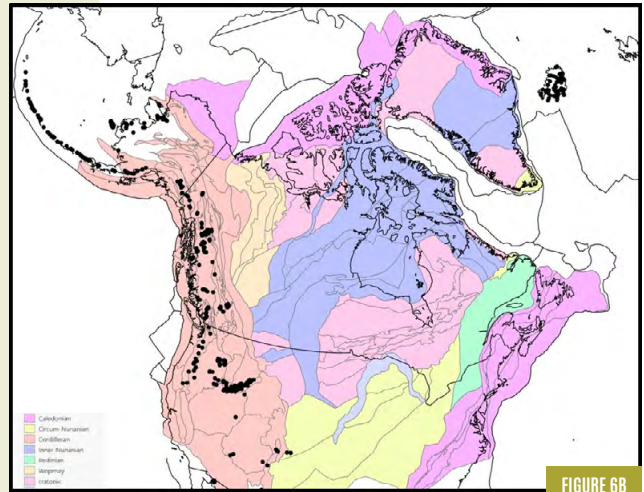NAD83 / Canada Atlas Lambert

FIGURE 5

FIGURE 6A

FIGURE 6B

isotherm is shallower (which it should be), but the difference in reported depth often exceeds +10 km. Blues are where the LithoRef18 450°C isotherm is deeper (which it should not be). Even here we observe results in excess of -10km.

Figures 6a and 6b reveal that, in general, the LithoRef18 depths to 450°C are deeper than the CDP models within the cratonic areas, and conversely, LithoRef18 is shallower in the younger orogenic regions on the eastern and western margins. It is not altogether surprising that in regions of very thick lithosphere (e.g., Superior Province) there is a large difference between CDP models and LithoRef18. In such cratonic and thick lithospheric regions, many CDP methods predict unrealistically shallow Curie depths, whereas LithoRef18 may underestimate subsurface temperatures given the relatively simplistic assumptions introduced in this model for radioactive heat production in continental crust (Afonso et al., 2019).

Spatial correlation of depth to 450°C with tectonic domain

Figures 6b and 7b reveal an underlying tectonic relationship that needs to be further explored. Firstly, it is observed that the dominant western trend of shallow 450°C anomalies is linked to the Cordilleran terrane, particularly within the accretionary complex and volcanic arc basement types. There is notably a second region where shallow "(i.e., < 15 km) anomalies are observed; this is in the eastern region of Canada. This region is a passive margin terrane, with a listed basement of Caledonian volcanic arc, a relatively old orogenic event.

Further work needs to be completed to determine whether the eastern anomaly is related to overprinting tectonics linked to the breakup and formation of the Atlantic. It's worth noting that Nova Scotia is highlighted as a region of sedimentary basin with moderate heat within the "Geothermal Energy Resource Potential of Canada" publication from the Geological Survey of Canada (Grasby, 2012). The depth to 450°C derived from the LithoRef18 models indicates that there is a lithospheric thermal anomaly within this region where additional analysis is required to better understand the origin of this thermal anomaly.

Spatial correlation of depth to 450°C with the location of conventional geothermal power plants and recent volcanics

Figures 7a and 7b highlight a positive correlation between both the distribution of powerplants and known recent volcanism in the western region of Canada and the United States with the shallow depth to 450°C isotherms derived from LithoRef18. Although this is not surprising, it does confirm the predicted spatial correlation using available data, while recognizing that it is likely biased towards hydrothermal and magmatic heat within the crust.

Conclusions

The study explores our first-order understanding of the depth to the 450°C isotherm based on a lithospheric model (LithoRef18) and independently derived temperatures from global models which interpret the depth to the CDP (i.e., 580°C).

The results revealed the following first-order observations:

Defining the depth to deep heat is notoriously difficult in the absence of constraining data. The models highlighted here reveal that all representations of the subsurface have limitations when predicting subsurface temperatures. One important thing to remember is that models are exactly that: models; they are not hard data points and carry a tremendous number of assumptions.

The 450°C isotherm from the LithoRef18 model is most shallow in the western Cordillera terrane, although shallow depths to the 450°C isotherm are also revealed in Nova Scotia in the Caledonian terrane.

Shallow depth of the 450°C isotherms correlates well with the distribution of recent volcanism and conventional geothermal power plants.

LithoRef 450°C isotherm depths are shallower than CDP within the western Cordillera and eastern Caledonian terranes, but deeper than CDP in the cratonic terrane. This highlights that CDP data may not be accurately reporting depth to CDP temperatures within regions of thick lithosphere and cratonic domains, or conversely, that LithoRef18 may be underestimating subsurface temperatures given the relatively simplistic assumptions introduced in this model for radioactive heat production in continental crust.

Comparisons of modelled and observed surface heat flow data reveal that the LithoRef18 model tracks the long-wavelength changes reasonably well. The fact that the long wavelength pattern of predicted and observed SHF match well indicates that high-frequency
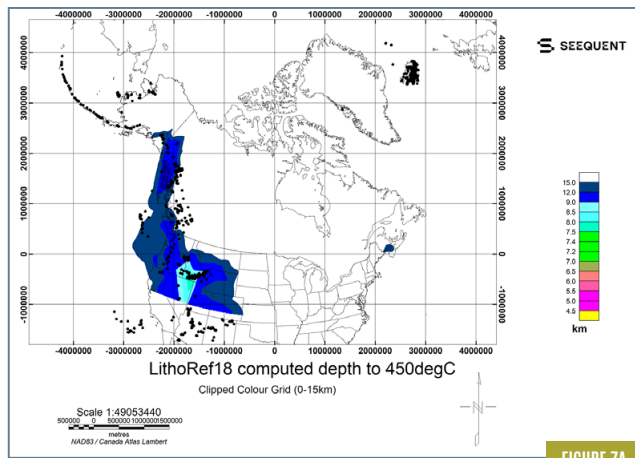
FIGURE 7A

FIGURE 7B

anomalies, revealed in the residual maps, are likely of shallow origin (for example, shallow water flow, small-scale magmatism, or hydrothermal activity).

This preliminary investigation allows us to consider some regions where more data and further studies are needed to understand and constrain the distribution of shallow heat within the crust and sedimentary basins of Canada. The model and analysis presented here could help non-profit advocacy groups, like the US-based Clean Air Task Force (CATF), Project InnerSpace, and the Canadian-based Cascade Institute, to better inform geothermal stakeholders in Canada of the potentially vast untapped geothermal resources within their provinces and country.
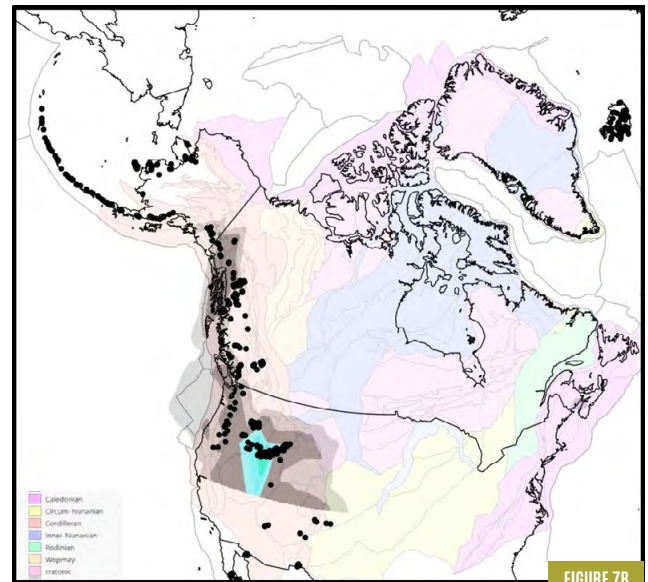
Acknowledgements

References

Afonso, J.C., Salajegheh, F., Szwillus, W., Ebbing, J. & Gaina, C., (2019). A global reference model of the lithosphere and upper mantle from joint inversion and analysis of multiple data sets, Geophys. J. Int., 217(3), 1602–1628, https://doi.org/10.1093/gji/ggz094

Angulo, A., and Vargas, C.A. (2022). Global distribution of the hydrocarbon Golden Zone. Marine and Petroleum Geology, Volume 144, https://doi.org/10.1016/j.marpetgeo.2022.105832.

Ball, P. J. (2021). A review of geothermal technologies and their role in reducing greenhouse gas emission. ASME Journal of Energy Resource Technologies, https://doi.org/10.1115/1.4048187

Ball, P.W., White, N.J., Maclennan, J., Stephenson, S.N., (2021). Global influence of mantle temperature and plate thickness on intraplate volcanism. Nature Communications, https://doi.org/10.1038/s41467-021-22323-9

Beard, J., and Jones, B., (2023). "The Future of Geothermal in Texas: The Coming Century of Growth & Prosperity in the Lone Star State." The Mitchell Foundation, https://energy.utexas.edu/research/geothermal-texas

CATF, (2022). Superhot Rock Energy: A Vision for Firm, Global Zero-Carbon Energy. CATF, https://cdn.catf.us/wp-content/uploads/2022/10/21171446/superhot-rock-energy-report.pdf

Fuchs, S., Norden, B., and International Heat Flow Commission, (2021). The Global Heat Flow Database: Release 2021, GFZ Data Services, https://doi.org/10.5880/fidgeo.2021.014

Garrity, C.P. and Soller, D.R. (2009). Database of the Geologic Map of North America— Adapted from the Map by J.C. Reed, Jr. and others (2005) Scale 1:5,000,000 USGS Data Series 424 Online linkage: http://pubs.usgs.gov/ds/424

Graham, I., Quigley, E., Janzwood, S., and Homer-Dixon, T., (2022). Deep Geothermal Superpower Canada's potential for a breakthrough in enhanced geothermal systems. The Cascade Institute, Technical Paper. https://cascadeinstitute.org/technical-paper/deep-geothermal-superpower/

Grasby, S. E., D. M. Allen, S. Bell, Z. Chen, G. Ferguson, A. Jessop, M. Kelman, M. Ko, J. Majorowicz, M. Moore, J. Raymond, and R. Therrien. (2012). "Geothermal Energy Resource Potential of Canada." Geological Survey of Canada 6914. https://publications.gc.ca/collections/collection_2013/rncan-nrcan/M183-2-6914-eng.pdf.

Grasby, S.E., Majorowicz, J., and Ko, M. (2009): Geothermal Maps of Canada, Geological Survey of Canada Open File 6167, 35p.

Grose, C. J. & Afonso, J. C., 2013. Comprehensive plate models for the thermal evolution of oceanic lithosphere, Geochemistry, Geophysics, Geosystems, 14(9), https://doi.org/10.1002/ggge.20232

Hasterok, D., Halpin, J.A., Collins, A.S., Hand, M., Kreemer, C., Gard, M.G., Glorie, S., (2022). New Maps of Global Geological Provinces and Tectonic Plates. Earth-Science Reviews, 104069, https://doi.org/10.1016/j.earscirev.2022.104069

Hickson, C.J., Raymond, J., Dusseault, M., Fraser, T., Huang, K., Marcia, K., Miranda, M., Poux, B., Fiess, K., Ferguson, G., Dale, J., Banks, J., Unsworth, M., Brunskill,

B., Grasby, S., and Witter, J., (2020). Geothermal Energy in Canada – Times Are "a Changing", GRC Transactions, Volume 44

Jessop, A. M., Morteza M. Ghomshei, Malcolm J. Drury, (1991). Geothermal energy in Canada, Geothermics, 20, 369-385, https://doi.org/10.1016/0375-6505(91)90027-S.

Li, C.-F. Lu, Y., Wang, J., (2017). A global reference model of Curie-point depths based on EMAG2. Sci. Rep. 7, 45129; https://doi:10.1038/srep45129

Müller, R.D., Sdrolias, M., Gaina, C., Roest, W.R., (2008). Age, spreading rates and spreading geometry of the world's ocean crust, Geochemistry, Geophysics, Geosystems, 9(4), https://doi.org/10.1029/2007GC001743

Potkins, M., (2023). Saskatchewan company greenlights Canada's first large-scale geothermal power plant A 25-megawatt facility should produce enough power for 25,000 households. Financial Post, online resource, accessed 10th Feb, 2023, https://financialpost.com/commodities/energy/geothermal-power-plant-deep-earth-energy

Razor Energy (2022). Canada's First Co-Produced Geothermal Power Project Is Fully Financed. Online resource, accessed February 16, 2023: https://www.globenewswire.com/en/news-release/2022/03/09/2400373/0/en/Canada-s-First-Co-Produced-Geothermal-Power-Project-Is-Fully-Financed.html

Uihlein, A., (2018): JRC Geothermal Power Plant Dataset. European Commission, Joint Research Centre (JRC) [Dataset] PID: http://data.europa.eu/89h/jrc-10128-10001

Why Join Mentoring365?

I started my career in Canada's Energy Industry 30 years ago and at that time, it was difficult to find a mentoring program and a mentor. I wanted a mentor who would share their professional experience and be a guide for me and my career. I eventually found mentors through a combination of perseverance and lots of coffee invitations!

As my career developed, I expanded my mentoring network. Some mentors helped me for a single issue, some for a couple of months, some for years. Several mentors became friends. I was so inspired by my mentors that I started mentoring myself. It was then that I realized why mentors mentor!

Working with mentees is amazing. It is so gratifying to watch a person grow and develop, and to forge new and long-lasting friendships. For me, mentoring is the best part of my career!

To my mentors, thank you for sharing your wisdom and knowledge, being a sounding board and giving me courage. To my mentees, thank you for your energy and enthusiasm, for asking questions and sharing your growth and learnings.

I am really excited about mentoring@CEGA's partnership with Mentoring365. Mentoring365 is a world class organization with 14 partners including NASA, GSA, AGU and SEG. Mentors and mentees are rewarded with exceptional opportunities to connect with Earth and Space Scientists from around the world and share wonderful life experiences!

Wendy Shier, P.Geo.

TOM BRADY AND THE VALUE OF A SAND GRAIN

Dallin Laycock, Rich Mackenzie, Erin Pemberton, Sean Fletcher, Paul M Bremner

INTRODUCTION

On February 1, 2023, legendary quarterback Tom Brady announced his retirement through a self-recorded video on social media. Several opportunistic fans recognized the location as a beach in Surfside, Florida (Figures 1 and 2), and quickly collected sediment samples from the locale to sell on eBay. Though the original listing was removed by eBay after reaching a value of $99,900, others managed to sell their jars of sand for various amounts up to $15,000. These events provide an opportunity to examine the relative value of sand resources and ask some crucial and interesting questions about the local geology, such as: What were these collectors actually buying? How did it get there? And was this sand, temporarily shaded by Tom Brady's shadow, actually the most valuable sand in the world?

THE VALUE OF SAND

In the petroleum industry, the value of sand has historically been attached to its ability to provide subsurface sandstone reservoirs with relatively high porosity and permeability. However, in recent years it has become apparent that the sand grains themselves are a valuable natural resource. Sand is the most-extracted solid material in the world with an estimated 50 billion tons consumed yearly (UNEP, 2022). Sand is used in almost all major industries: the construction industry as an aggregate; the petroleum industry as a hydraulic fracturing proppant; the tech industry melts it down to make glass and silicon, and obviously the tourism industry in coastal environments relies heavily on sandy beach fronts such as the ones observed at Surfside, Florida (Figure 2).

Some governments, such as in Puerto Rico, have even reported sand theft (Rodriguez, 2017). Adding complication is the fact that this extensive sand extraction is unregulated. The United Nations Environmental Programme (UNEP, 2022) has proposed more regulation, tracking of global sand usage, and incentives for finding sand alternatives in various projects. The extensive use of sand, combined with the effects of anthropogenic alteration of shorelines has limited sediment supply in many natural environments (Runyan and Griggs 2003; Anderson et al., 2014; Hackney et al., 2021). As a result, sand is more important and valuable than ever before. The average price of construction-grade sand has increased roughly 50% in the last 12 years (Figure 3). Though, even with this increase, construction-grade sand can still cost as low as $11 USD per metric ton, a price that continues to fuel heavy consumption.

Not all sand is valued the same, and a wide range exists. For example, construction quality sand sells for a relatively low price compared to $10,000 USD/metric ton for specialized quartz sand used by the tech industry (Beiser, 2018). Indeed, that's a high price, but with price tags of $15,000 to $99,900 for a jar of sand, the Tom Brady retirement sand from Surfside is a strong candidate for the world's most valuable sand. With such a high cost, what would be the approximate price per sand grain? And what did people actually buy for that exorbitant price? Let's break this down, first by price per sand grain.

To calculate the price per grain of sand, we must first estimate how many grains of sand fit inside that mason jar. There are many ways of doing this calculation, but we will use the following methodology: The jar in the image appears to be a 16 oz mason jar, or approximately 473 mL of volume. At this point, several assumptions are needed to proceed: 1) We will assume the grains are packed in a hexagonal close packing configuration, yielding about 40% porosity. 2) We assume all the sand grains are medium-grained. 3) We assume all the sand grains approximate a spherical shape with radius of 0.165 mm.

FIGURE 1:

A) Image from Tom Brady's social media post announcing his retirement (via TomBrady/IG). In this image, and throughout the video, sand can be seen under him (white arrow), suggesting he is at the edge of the vegetation at the eastern edge of the beach. The buildings in the background can be used as a reference for his location.

B) Image from the eBay listing for the jar of sand that generated bids of $90,900 (via SportsCenter/IG). Red arrows indicate common buildings between the images to assist with the location verification.
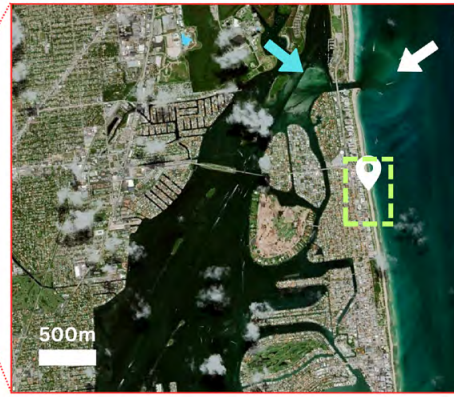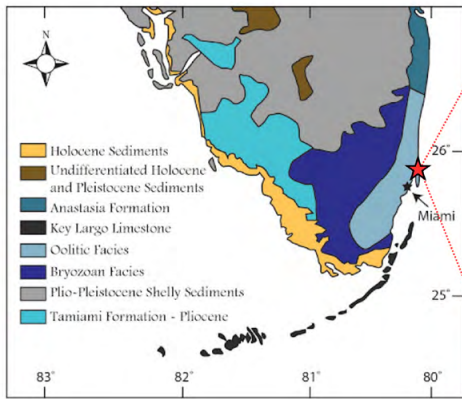
FIGURE 2: Geologic map of southern Florida (modified from Neal et al., 2008). Inset map to the right shows the location of the video recording and where the sand was collected (white pinpoint). The coordinates of this point are 25.8835471, -80.1206069. The image also shows the barrier island, as well as flood and ebb tidal deltas (blue and white arrows respectively) on either side of the artificially created Haulover Inlet. The green dashed box shows the location featured in Figure 5.

The volume of a sphere can be calculated with the following formula:

$$V = 4/3\ \pi r^3$$

With a radius of 0.165 mm, the volume of each sand grain becomes 0.0192 mm³. The jar's volume of 473 mL then converts to 4.73×10^5 mm³. Using these components, along with the assumed porosity of 40%, the estimated number of sand grains in this jar is:

$$(4.73 \times 10^5\ mm^3 (\text{volume of jar}))/((0.0192\ mm^3\ \text{grain-1})) \times (1-0.4) = 14{,}781{,}250\ \text{sand grains}.$$

At $99,900 for the entire jar, the price works out to $0.0068 USD per grain. With the value of this sand established, let's address the second question: "What were these people actually bidding on?"

THE SAND OF SOUTH FLORIDA

Surfside is located on a barrier island extending off the southeastern portion of the Florida peninsula. The location is just south of an inlet with visible flood and ebb tidal deltas (Figure 2). Predominantly, this is a carbonate system overtopped with coral and shell fragments from the ocean, as well as inland erosion and sediment transport to the coast contributing to the overall sediment load. Sand migrates north-to-south,

FIGURE 3: Average price of construction-grade sand and gravel in the US from 2010 to 2022 (statistica.com).

meaning the health of the barrier island system depends upon the constant delivery of sand from the north. Visible on satellite imagery, a series of jetties and seawalls along the shoreline limit sediment delivery to this barrier island. There are five inlets with artificial seawalls within 75 km to the north of the Tom Brady retirement location. The satellite imagery shows that these structures are trapping sand and preventing its natural migration, as apparent by sand-starved beaches to the south of the structures (Figure 4).

Perhaps the best place to visualize the importance of sand is at the Kennedy Space Center at Cape Canaveral, FL, where the sand on the beach protects NASA's access to space (Figure 5). Cape Canaveral relies on constant sand delivery via alongshore migration from the north. Historical satellite images show sediment migrating around the tip of the cape, being deposited on the shoreline to the south. This results in net erosion north of the cape, and net deposition along the south (Adams, 2018; Mackenzie et al., 2023).

If sediment delivery were to be diminished, erosion on the north side of the cape would accelerate significantly. The same sediment budget dynamics exists in other locations along the Florida coastline, although less visible than Cape Canaveral. As such, the barriers to sediment migration in South Florida, combined with continued sea-level rise can be devastating to these shallow marine environments. This has prompted extensive beach renourishment projects to protect local beaches and maintain their appeal as tourist destinations.

Beach sand in South Florida was already valuable, as local governments invest millions of dollars keeping their beaches looking pristine. In 2019, Miami-Dade County reported that it had funding of $158.3M USD for this beach renourishment project (refer to the Miami-Dade County, Surfside Beach Renourishment Project report). While this is an expensive
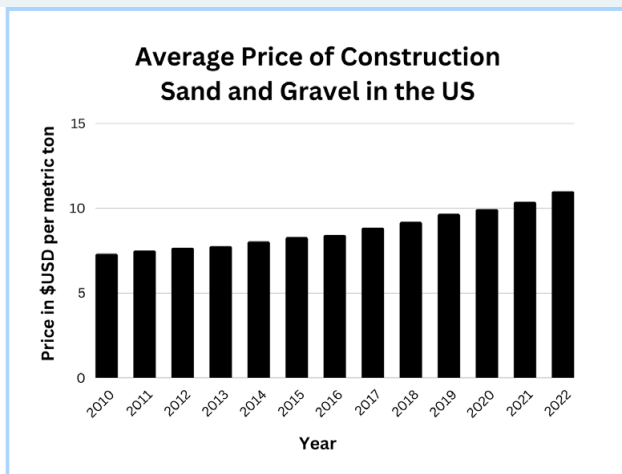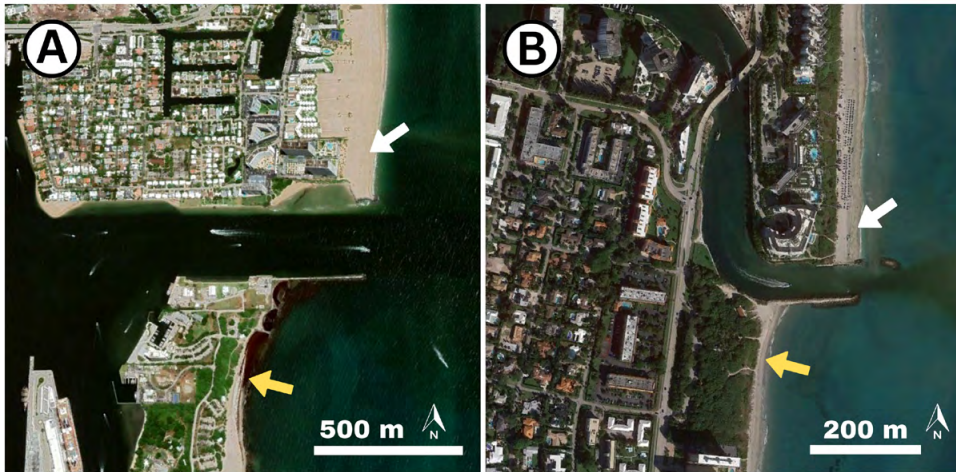
FIGURE 4: Contrast between beaches on the proximal side (white arrows) of jetties vs the distal side (yellow arrows) where beaches are artificially starved of sediment migrating south along the beach. Location A) 26.093958, -80.104335, approximately 24 km to the north of the Tom Brady retirement location. Location B) 26.3363573, -80.0722546, approximately 50 km to the north of the Tom Brady retirement location.

project, it pales in comparison to the potential loss of tourism dollars, as Miami-Dade County collects around $10-20 USD billion per year in revenue from tourism. Pristine beaches are a major component of the region's tourist attractions.

Anthropogenic barriers to sediment migration have left this beach in Surfside starved for sediment and prone to damage from storms and continued sea-level rise. To combat these effects, local governments have undertaken beach alimentation efforts designed to replace the sediment that is continuously removed by natural sedimentary processes. These usually involve dredging sand from nearshore environments and placing it back on the beach, where tractors spread it out and let nature resume its natural processes (Figure 6). If this is not performed, the beach would continue to erode and eventually threaten the town. As a result, the "Tom Brady sand" was not deposited there by natural sources, but rather by a fleet of heavy machinery contracted by local governments to maintain tourism (Figure 6 inset).

The methods of sand nourishment in South Florida are relatively inefficient. Sand is dredged offshore, trucked onto the beach with large dump trucks, and re-distributed with bulldozers. From there, the natural process of wave energy reworks, transports, and ultimately removes the sand. In an effort to preserve a natural environment as much as possible, local governments (including that of Surfside) have established specifications for nourished sand. All sand must meet the following specifications (as per the Miami-Dade County, Surfside Beach Renourishment Project report):

- Sand must be predominantly $CaCO_3$ or quartz, with no more than 5% comprising other minerals.
- Average grain size between 0.30 mm and 0.55 mm, with standard deviation between 0.50 phi and 1.75 phi (poorly sorted to moderately well sorted).
- Silt and clay content less than 5% of total volume.
- 95% of the sand must pass through the 4.76 mm sieve, 99% must pass through the 9.51 mm sieve, and 100% must pass through the 19.0 mm sieve.
- Sand must be naturally created. Crushed rock constitutes manufactured sand and is prohibited.
- Sand color must resemble that of the existing beach.

These requirements provide a detailed description of the contents of the Tom Brady sand. In addition to providing the information on composition, they have also provided information on the cost of obtaining sand that meets this description. In 2019 this sand had costs ranging from $50 to $65 per cubic yard. To convert the price per cubic yard to metric tonnes, we use the following calculation:

Each cubic yard is equivalent to 764,555 cm^3. Given a sand density of 1.52 gm/cm^3, we multiply them together to get a weight of 1162.12 kg, which we divide by 1000 to get 1.162 metric tonnes for each cubic yard. Using the higher end of the price spectrum for the Miami beach sand, we get $65/1.162 tons, which works out to a price of approximately $56/metric ton. This is significantly higher than the $11 per metric ton of sand used in construction projects, which makes sense given its specific requirements. How does this compare to the price of the Tom Brady sand? The jar of sand seen on eBay appears to have been a 16 oz mason jar. One cubic yard contains 25,852.7 fluid ounces, or 4,308.8 16 oz mason jars. If each jar is worth $99,900, then one cubic yard works out to $430,449,120, which works out to $370,438,141 per metric ton of sand. We can then conclude that Tom Brady's temporary presence multiplied the value of this artificially placed sand by over 6.5 million times!

CONCLUSION

The exorbitant sums of money paid for artificially emplaced sand, which skyrocketed in value when it temporarily contacted the backside of Tom Brady, has allowed us to examine the current state of sand resources around the world. In what is likely the most valuable sand in the world, we have calculated the "Tom Brady sand" to be worth approximately $0.0068 USD per grain, or $370,438,141 per metric ton, compared to $11 per ton in construction projects. However, it is this relatively cheap price for sand (that has not been graced by a superstar) that continues to fuel the excessive consumption of this increasingly scarce resource. Repercussions of this impending sand shortage will be increasingly problematic for a variety of industries and locations, including the very spot that generated the sand on which Tom Brady sat for his latest retirement announcement.

FIGURE 5 (ABOVE): Aerial photography from 1943 of Cape Canaveral showing that Launch Complex LC-39A was built on sand deposited by a flood tide delta. It also shows the proximity of the shoreline, and how erosion of the shoreline could impact the launch infrastructure (Modified from Mackenzie et al. 2023).

FIGURE 6 (BELOW): Time slices of the Tom Brady retirement location (red pinpoint). Initially this beach was approximately 25-m wide. In December of 2019, beach nourishment construction can be seen at the south side of the image (panels B and C). By February of 2020, the widening of the beach had progressed to the north of the Tom Brady retirement location (see panel D, green arrow). By March of 2020 (panel E), the beach is more than double the width seen in panel A.
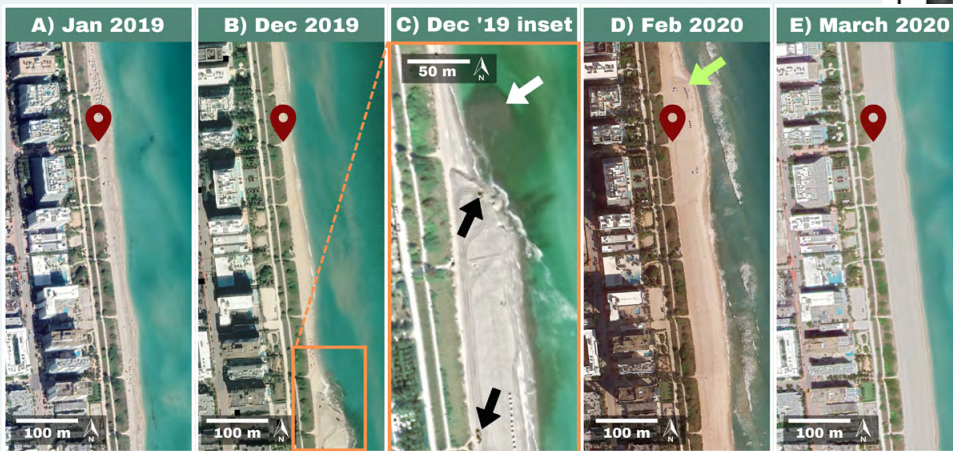
As sea-level continues to rise, and human development continues to hinder sediment delivery to the coast, beaches like those found in Surfside, Florida, will have to develop solutions to address their sand supply issues. Is perpetual sand nourishment sustainable in the long-term? Are sea-walls, jetties, and other inhibitors to sediment movement worth the damaging effects they have on coastlines? Are there more sustainable solutions to protecting coastlines? These are important issues in which geologists will have a tremendously important role. Geologists will be crucial for helping resolve sediment budgets and evaluating sediment migration pathways in these sensitive depositional environments. In addition, geologists can help identify sustainable replacements for limited sand resources around the world. And hopefully, Tom Brady's next retirement announcement will feature another geologically interesting location.

REFERENCES

Adams, P.N. (2018). Geomorphic origin of Merritt Island-Cape Canaveral, Florida, USA: A paleodelta of the reversed St. Johns River? Geomorphology. v. 306. p. 102-107.

Anderson, J. B., Wallace, D. J., Simms, A. R., Rodriguez, A. B., & Milliken, K. T. (2014). Variable response of coastal environments of the northwestern Gulf of Mexico to sea-level rise and climate change: Implications for future change. Marine Geology, 352, 348-366.

Beiser, V. (2018). The Ultra-Pure, Super-Secret Sand That Makes Your Phone Possible. Wired Magazine. https://www.wired.com/story/book-excerpt-science-of-ultra-pure-silicon/

Hackney, C. R., Vasilopoulos, G., Heng, S., Darbari, V., Walker, S., & Parsons, D. R. (2021). Sand mining far outpaces natural supply in a large alluvial river. Earth Surface Dynamics, 9(5), 1323-1334.

Mackenzie, R., Bremner, P., Laycock, D., Fletcher, S., Pemberton, E. (2023). Visualizing Sedimentological Variability Near Vulnerable NASA Infrastructure at Cape Canaveral, FL and Wallops Island, VA. Geoconvention 2023.

Neal, A., Grasmueck, M., McNeill, D. F., Viggiano, D. A., & Eberli, G. P. (2008). Full-resolution 3D radar stratigraphy of complex oolitic sedimentary architecture: Miami Limestone, Florida, USA. Journal of Sedimentary Research, 78(9), 638-653.

Rodriguez, R.W. (2017). Sand and Gravel Resources of Puerto Rico. USGS Fact Sheet. https://pubs.usgs.gov/fs/sand-gravel/

Runyan, K., & Griggs, G. B. (2003). The effects of armoring seacliffs on the natural sand supply to the beaches of California. Journal of coastal research, 336-347.

UNEP. (2022). Sand and sustainability: 10 strategic recommendations to avert a crisis. GRID-Geneva, United Nations Environment Programme, Geneva, Switzerland; URL : https://unepgrid.ch/en/resource/2022SAND

Miami-Dade County, Surfside Beach Renourishment Project report (2019). https://townofsurfsidefl.gov/docs/default-source/newsletters/miami-dade-county-beach-renourishment-project.pdf?sfvrsn=8cb45c94_4

WRAP UP

Building from the momentum of last year's core conference, our conference planning committee hit the ground running in September to begin organizing this year's core conference. Our theme "Let the Rocks Talk: The Past, Present and Future of Energy Resources" aimed to acknowledge that core work was essential to unlocking historic plays, is fundamental in today's exploration and development, and will continue to be integral in the ever-evolving future landscape of energy resources.

CAROLYN FURLONG AND SCOTT MACKNIGHT
2023 CSPG Core Conference Co-Chairs

This year we had a fantastic line-up of 19 presenters from industry, government and academia that provided presentations covering three diverse themes including energy's new frontier, sedimentology and reservoir characterization, and Alberta's hot plays. Over two days we had presentations that investigated hydrogen storage in salt caverns, lithium distribution, the deepest borehole from the Whitehorse Trough in the Yukon, ichnology from a core from offshore Nova Scotia, placer gold potential of the Mannville Group in Saskatchewan, pore system variability from the Duvernay Formation, and so much more! For the first time, the core conference also included a keynote talk, by Dr. Brad Hayes, who provided a conference-opening presentation entitled "21st Century Energy Transition: The Global Challenge of our Time," which highlighted the need for core work during our current energy transformation. We are so grateful for the support we received from our presenters who gave us not only their precious time but were

also unstinting with their knowledge and diverse views on our ever evolving industry.

Turnout was exceptional and exceeded our expectations as we attracted over 530 delegates. It was nice to see faces that were familiar and new. The positive momentum from the conference spilled over into the Meltdown, which was held offsite at Kilkenny's, where we continued to catch up, talk about rocks, and celebrate the end of a successful conference.

Congratulations to Joel Collins and Pak Wong who won the Pemberton Award for best overall presentation. Their presentation on the Beaverhill Lake Group highlighted the importance of utilizing core to understand carbonate stratigraphy across the basin and was a wonderful preview of their upcoming contributions within the 2027 Western Canada Sedimentary Basin Atlas update. Drew Brown

with Hilary Corlett, Murray Gingras, Tom Kibblewhite, Fiona Whitaker and John-Paul Zonneveld as co-authors, won the Baillie Award for best student presentation and the $1000 dollar prize. Drew's presentation on carbonate microfacies from the Abu Dhabi coastal sabkha integrated various datasets along a transect through a modern sabkha environment to better understand similar carbonate sequences in the rock record.

This conference would not have been possible without the support of our sponsors and advertisers. We would like to thank Tourmaline Oil, our title sponsor, for its continued support, our program book sponsor APEGA and our student sponsor ProGeo Consultants, who covered the cost of entry for 20 student delegates. We would like to thank the session sponsors: AGAT, Spur Petroleum Ltd. and Canadian Discovery Ltd., as well as the poster board sponsors: Vidence Inc., Imperial Oil and ConocoPhillips. Core Laboratories sponsored the delicious snacks at the coffee break and Stratum

THANK YOU TO THOSE WHO ATTENDED THE CONFERENCE

We look forward to next year's conference and the opportunities it presents.

Reservoir/AGAT sponsored the BBQ lunch. ROGII Inc. and Chinook Consulting Services returned as sponsors for the Core Meltdown. We would also like to thank the AER Core Research Centre for pulling core and giving us access to their world-class facility, as well as the BCER core facility and Saskatchewan Subsurface Geological Lab for allowing access to borrowed core.

It has been a real team effort to pull together the 2023 conference. We had an amazing group of volunteers: Nick Ayre from Strathcona Resources, Christa Williams from Canadian Discovery, Daniela Becerra from Schlumberger, James Burr from Spur Petroleum, Lauren Eggie from Imperial Oil, Ozzy Ofoegbu from Cenovus, Jerome Biollo and Rob Paul, our resident rock enthusiasts, Mark Radomski from Cenovus, Celine Chow from Saturn Oil and Gas Inc. and Cole Ross from Spur Petroleum. We would also like to take the opportunity to thank Shaelyn Brown and the staff at the CEGA office for helping to put together this event. A HUGE thank-you to

GO TAKE A HIKE... TOGETHER!
August 19 • Helen Lake

Join Astrid Arts and Mark Mallamo for this moderate hike on the Helen Lake Trailhead!

TO REGISTER PLEASE
CLICK HERE

Canstrat Data and the Seamless Unison with Machine Learning
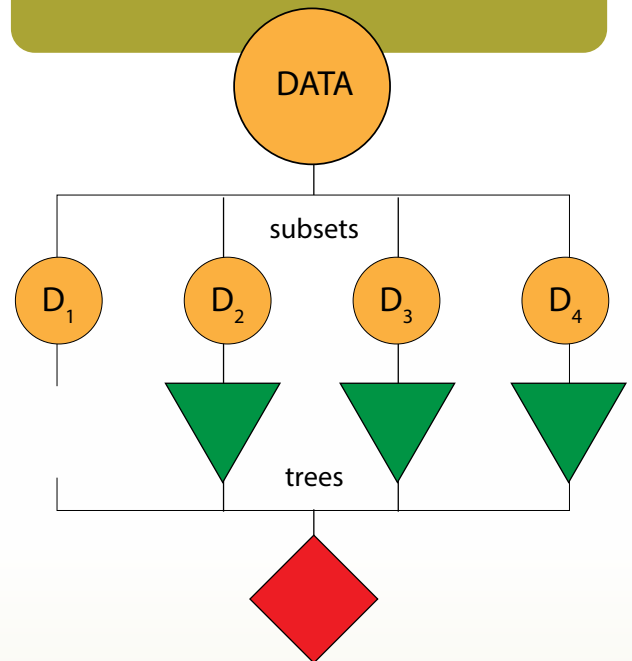
Aleksandra Tatomirovic

The oil and gas industry has been greatly impacted by advancements in technology, including the use of machine learning. Machine learning, a type of artificial intelligence (AI), is the process by which machines can learn and improve upon their own performance without being explicitly programmed. The vast amounts of data generated by the oil and gas industry can now be analyzed through machine learning algorithms to optimize operations, minimize costs, and increase efficiency. With the help of machine learning, the oil and gas industry is embracing digitalization and transforming itself into a smarter, more sustainable energy sector. In addition to improving the efficiency of data analysis, machine learning can also help to identify previously unknown relationships between different variables in the data. This can lead to a deeper understanding of well performance and can inform the development of new strategies for optimizing production. However, it is important to note that while machine learning is a powerful tool, it is not a solution. Properly training and validating machine learning models is crucial in order to ensure that the results are accurate and trustworthy.

Random Forests
Needs little tuning and provides prediction probability. In addition, they do extremely well in higher dimensions and provide feature importance.

DATA

subsets

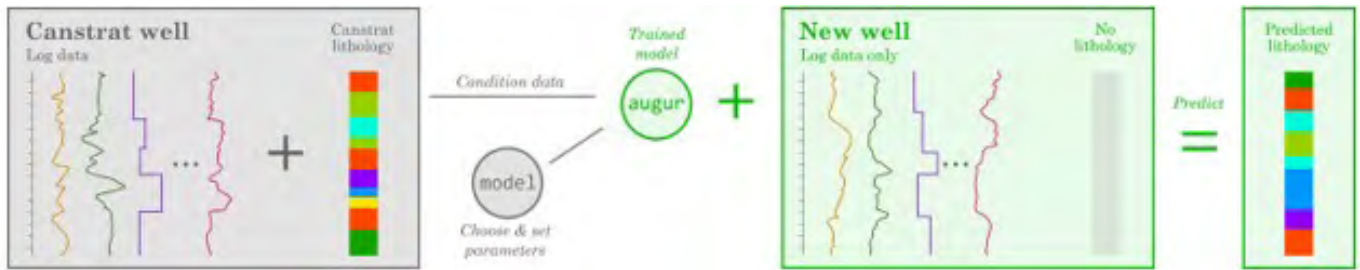D_1 D_2 D_3 D_4

trees

Canstrat LAS well cuttings data is ideal for machine learning purposes because it provides a rich and diverse dataset that can be used to train machine learning algorithms. The data is collected during the drilling process and provides information on the lithology, texture and structure of the rocks being drilled, including the mineralogy and grain size. The diversity of the Canstrat LAS well cuttings data makes it an excellent candidate for machine learning, as machine learning algorithms require large and diverse datasets to be trained effectively. With the growing availability of large amounts of data from the oil and gas industry, machine learning has become an increasingly popular method for analyzing and interpreting data.

Canstrat LAS well cuttings data is typically available in a standardized format, which makes it easier to analyze and compare across different wells and formations. This standardization makes it possible to develop machine learning models that can be applied across a wide range of data, providing valuable insights into subsurface geology and reservoir properties. Machine learning algorithms can be trained on Canstrat LAS well cuttings data to identify patterns and relationships between different rock types and properties, which can be used to predict rock properties such as porosity and permeability. These predictions can then be used to optimize drilling and completion operations, reduce costs, and improve production efficiency.

Another advantage of using Canstrat LAS well cuttings data for machine learning is that it can be combined with other types of well data, such as well logs and seismic data, to create more accurate and comprehensive models of the subsurface geology. By combining these different data sources, machine learning algorithms can provide a more complete understanding of the subsurface geology and reservoir properties, thus improving exploration and production results.

One common pre-processing step is to convert the Canstrat LAS well cuttings data into a numerical format that can be used to train machine learning algorithms. This can be done using techniques such as one-hot encoding, which converts categorical variables, such as lithology type, into binary features that can be used by the algorithm. Continuous variables, such as grain size and mineralogy, can be normalized and standardized to ensure that they have the same scale and range. Once the data has been pre-processed, it is typically split into training, validation, and testing sets. The training set is used to train the machine learning algorithm, while the validation set is used to tune the algorithm's hyperparameters, such as the learning rate and regularization. The testing set is used to evaluate the performance of the trained algorithm on unseen data.

The machine learning algorithm is then trained using a variety of supervised or unsupervised learning techniques, such as regression, classification, clustering, or deep learning. For example, a regression model can be trained to predict porosity or permeability from the Canstrat LAS cuttings data, while a classification model can be trained
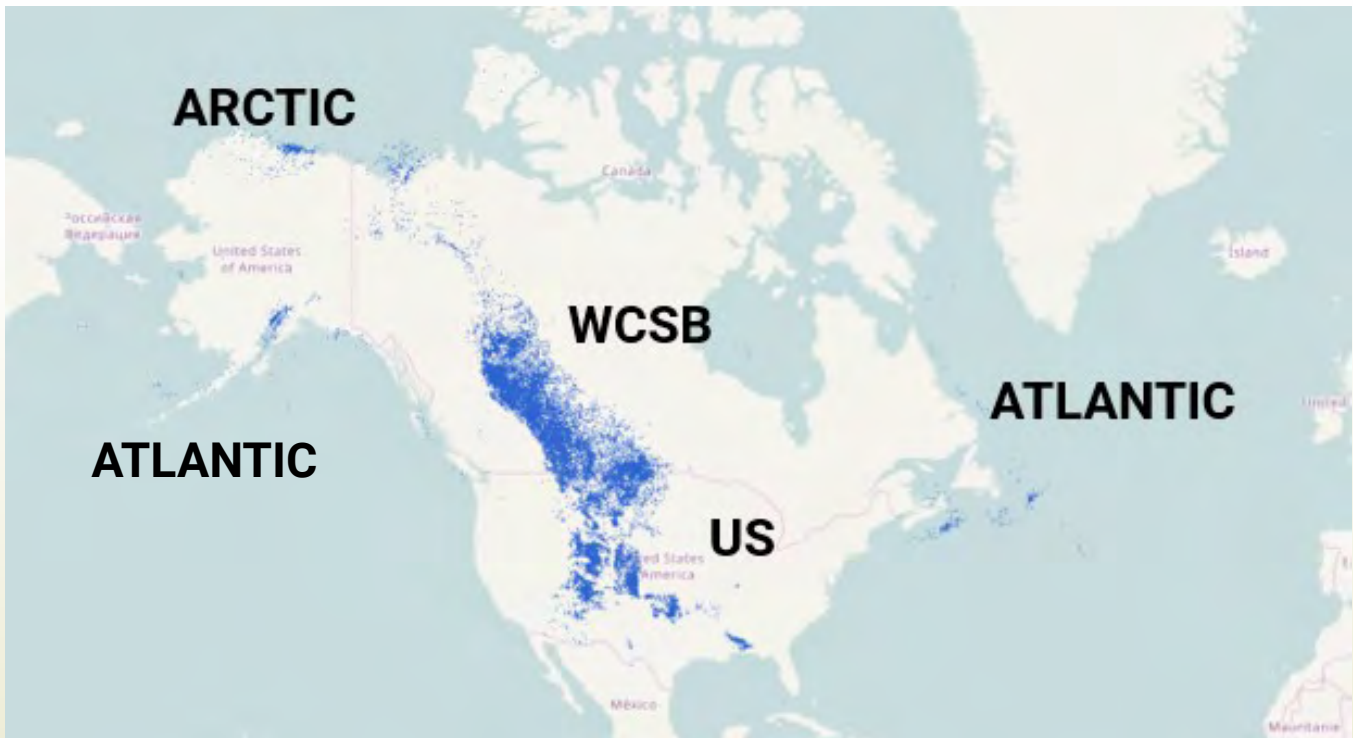
WELL WITHOUT VALIDATION AT HIBERNIA. DEVELOPMENT WELL B-16 NO 9.
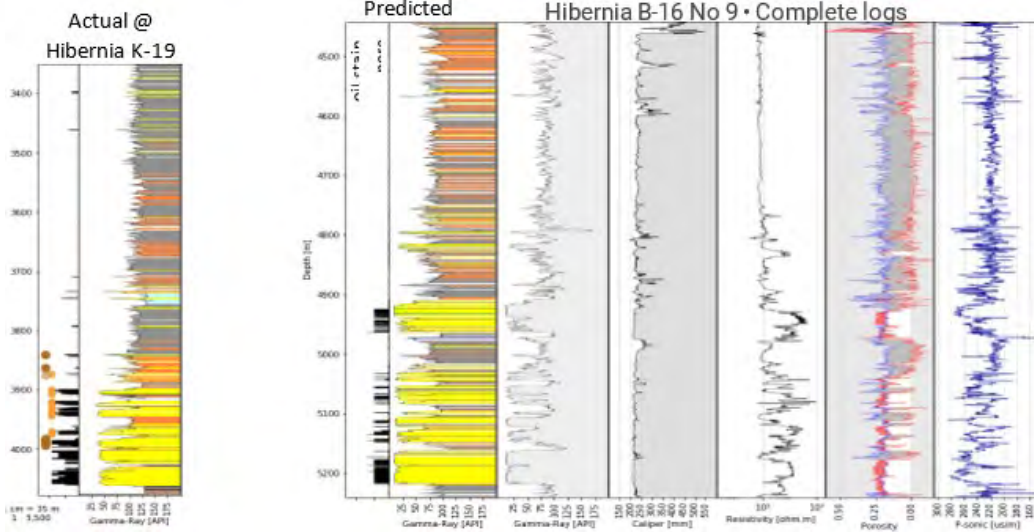
CANSTRAT'S INTERACTIVE LOGSOURCE DATABASE HOUSES ALL 35,000 WELLS ACROSS NORTH AMERICA. LOGSOURCE IS THE SOURCE OF ALL THE DATA THAT WAS USED FOR THE PURPOSES OF MACHINE LEARNING.

to identify different lithology types. During the training process, the machine learning algorithm learns to identify patterns and relationships between the input features and the target variable, using techniques such as gradient descent to optimize the model's parameters. The model's performance is evaluated using metrics such as mean squared error or accuracy, and the hyperparameters are tuned to improve the model's performance on the validation set. Once the algorithm has been trained and optimized, it can be used to make predictions on new Canstrat LAS well cuttings data, providing valuable insights into the subsurface geology and reservoir properties. These predictions can be used to optimize drilling and completion operations, reducing costs, and improving production efficiency.

In conclusion, machine learning algorithms can be trained using Canstrat LAS well cuttings data by pre-processing the data, splitting it into training, validations, and testing sets, and using supervised or unsupervised learning techniques to train the model. The algorithm learns to identify patterns and relationships between the input features and the target variable, and the model's hyperparameters are tuned to improve its performance. Once trained, the algorithm can be used to make predictions on new Canstrat LAS well cuttings data, providing valuable insights into the subsurface geology and reservoir properties.

THANK YOU TO ALL THE CEGA SPONSORS

TITANIUM

CSPG FOUNDATION

TOURMALINE OIL CORP.

Alberta Energy Regulator

PLATINUM

STRATUM RESERVOIR

GOLD

APEGA

geoLOGIC SYSTEMS

SILVER

CHINOOK CONSULTING SERVICES

Core Lab RESERVOIR OPTIMIZATION

AGAT Laboratories

ARC RESOURCES LTD.

ROGII

BIRCHCLIFF ENERGY

Imperial

BRONZE

Canadian Discovery Ltd.

WELLSITE SUPERVISION PROGEO LAB & ANALYTICS GEOSTEERING

Waterline

Matrix Solutions Inc. ENVIRONMENT & ENGINEERING

SPUR PETROLEUM LTD

GLJ

Freehold ROYALTIES LTD.

ALT Advanced Logic Technology

Crescent Point

Spectrum geosciences

ConocoPhillips Canada

CORPORATE SUPPORTERS

Belloy Petroleum Consulting

Cabra Consulting Ltd.

SeisWare

Spartan Delta Corp.

Pason Systems Inc.

McDaniel & Associates Consultants Ltd.

Canamera Coring

RIGSAT Communications

Barreleye Tools

Schlumberger Technology Corporation

Earth Signal Processing Ltd.

Pulse Seismic Inc

Sigma Explorations

Whiskey Jack Resources

Advanced Logic Technology

Santos Inc.

Eucalyptus Consulting

As of July 1st, 2023.

UPCOMING
EDUCATION
COURSES

Regional Geology of the Montney Resource Play: Western Canada Sedimentary Basin
September 25-28, 2023

Instructors:
Thomas F. Moslow, Ph.D, P.Geol. and John-Paul Zonneveld, Professor

Member Rate: $2600
Non-Member Rate: $3400

Sequence Stratigraphy and Reservoir Characterization of Non-marine, Marginal Marine, and Incised Valley Deposits: Examples from the WCSB
October 25-27, 2023

Instructor:
Brian Zaitlin, Ph.D., P.Geol., CPG.

Member Rate: $2400
Non-Member Rate: $3000

Gas Reservoir Engineering for Geoscientists
November 8, 2023

Instructor:
Kamal Malick, P. Eng.

Member Rate: $575
Non-Member Rate: $775

Oil Reservoir Engineering for Geoscientists
November 7, 2023

Instructor:
Kamal Malick, P. Eng.

Member Rate: $575
Non-Member Rate: $775

REGISTER NOW
cspg.org/education